Towards a satellite formaldehyde – in situ hybrid estimate for organic aerosol abundance

Jin Liao[1,2], Thomas F. Hanisco[1], Glenn M. Wolfe[1,3], Jason St. Clair[1,3], Jose L. Jimenez[4,5], Pedro Campuzano-Jost[4,5], Benjamin A. Nault[4,5], Alan Fried[6], Eloise A. Marais[7,*], Gonzalo Gonzalez Abad[8], Kelly Chance[8], Hiren T. Jethva[1,2], Thomas B. Ryerson[9], Carsten Warneke[9,5], Armin Wisthaler[10,11]

[1]Atmospheric Chemistry and Dynamic Laboratory, NASA Goddard Space Flight Center, Greenbelt, MD, USA
[2]Universities Space Research Association, GESTAR, Columbia, MD, USA
[3]University of Maryland Baltimore County, Joint Center for Earth Systems Technology, Baltimore, MD, USA
[4]Department of Chemistry, University of Colorado, Boulder, Colorado, USA
[5]Cooperative Institute for Research in the Environmental Sciences, University of Colorado, Boulder, Colorado, USA
[6]Department of Atmospheric and Oceanic Sciences, University of Colorado Boulder, Boulder, Colorado, USA
[7]School of Geography, Earth and Environmental Sciences, University of Birmingham, UK
[8]Harvard-Smithsonian Center for Astrophysics, Cambridge, Massachusetts, USA
[9]NOAA Earth System Research Laboratory (ESRL), Chemical Sciences Division, Boulder, CO, USA
[10]Department of Chemistry, University of Oslo, Oslo, Norway
[11]Institute for Ion Physics and Applied Physics, University of Innsbruck, Innsbruck, Austria
[*]now at Department of Physics and Astronomy, University of Leicester, Leicester, UK

Correspondence email: jin.liao@nasa.gov

Abstract

Organic aerosol (OA) is one of the main components of the global particulate burden and intimately links natural and anthropogenic emissions with air quality and climate. It is challenging to accurately represent OA in global models. Direct quantification of global OA abundance is not possible with current remote sensing technology; however, it may be possible to exploit correlations of OA with remotely observable quantities to infer OA spatiotemporal variability. In particular, formaldehyde (HCHO) and OA share common sources via both primary emissions and secondary production from oxidation of volatile organic compounds (VOCs). We examine OA-HCHO correlations using data from summer-time airborne campaigns investigating biogenic (NASA SEAC^{4}RS and DC3), biomass burning (NASA SEAC^{4}RS) and anthropogenic conditions (NOAA CalNex and NASA KORUS-AQ). In situ OA correlates well with HCHO ($r = 0.59 - 0.97$) but the slope and intercept of this relationship vary with chemical regime. For biogenic and anthropogenic regions, the OA-vs-HCHO slope is higher in low NO_x conditions, where HCHO yields are lower and aerosol yields are likely higher. The OA-vs-HCHO slope of wild fires is more than 9 times higher than that associated with biogenic and anthropogenic sources. Near-surface OA over the continental US are estimated by combining observed in situ relationships with HCHO column retrievals from NASA's Ozone Monitoring Instrument (OMI). HCHO vertical profiles used in OA estimates are from climatology a-priori profiles in the OMI HCHO retrieval or output of specific period from a newer version of GEOS-Chem. We evaluate these OA estimates against OA observations from the US EPA IMPROVE network and simulated OA from the GEOS-Chem global chemical transport model. The OA estimates compare well with

IMPROVE data obtained over summer months (e.g. slope = 0.60-0.62, r = 0.56 for August 2013), comparable to intensively validated GEOS-Chem performance (e.g. slope = 0.57, r = 0.56) and superior to the correlation with satellite-derived total aerosol extinction (r = 0.41). This also indicates that OA estimates are not very sensitive to HCHO vertical profiles and that a priori profiles from OMI HCHO retrieval are similar to that from the newer model version in estimating OA. Improving the detection limit of satellite HCHO and expanding in situ airborne HCHO and OA coverage in future missions will improve the quality and spatiotemporal coverage of this OA estimate, potentially enabling constraints on the global OA distribution.

1. Introduction

Aerosols are the largest source of uncertainty in climate radiative forcing (IPCC 2013; Carslaw et al., 2013) and also decrease atmospheric visibility and impact human health (Pope 2002). Organic aerosols (OA) comprise a large portion (~50%) of submicron aerosols (Jimenez et al., 2009; Murphy et al., 2006; Shrivastava et al., 2017), and this fraction will grow with continued decline in SO_2 emissions (Attwood et al., 2014; Marais et al., 2017; Ridley et al., 2018). In addition, OA serve as cloud condensation nuclei (CCN) and affect cloud formation and climate radiative forcing. Research even found that the inclusion of phase-separation effects from organic material into cloud droplet activation thermodynamics in climate models can lead to important changes in CCN concentrations (Ovadnevaite et al., 2017). OA components also have adverse health effects (e.g. Walgraeve et al., 2010) and contribute significantly to regional severe haze events (e.g. Hayes et al., 2013). Finally, because the response of temperature to changes in climate forcing is non-linear (Taylor and Penner, 1994) and the forcing by aerosols has strong regional character (Kiehl and Briegleb, 1993), it is necessary to separate out different climate forcing components to accurately forecast the climate response to changes in forcing.

It is challenging to accurately represent OA in global models. Chemical transport models (CTMs) often under-predict OA (e.g., more than a factor of 2 lower OA near the ground) compared to observations, and model-to-model variability can exceed a factor of 100 in the free troposphere (Tsigaridis et al., 2014; Heald et al., 2008; Heald et al., 2011). Fully explicit mechanisms (e.g. Lee-Taylor et al., 2015) attempt to capture the full OA

chemical formation mechanisms, but it is too computationally expensive to apply these mechanisms to OA formation in global CTMs at a useful resolution. For computational efficiency, 3-D models such as GEOS-Chem include direct emissions of primary OA (POA) and either represents secondary OA (SOA) formation by lumping SOA products according to similar hydrocarbon classes (Kim et al., 2015) or based on the volatility of the oxidation products (Pye et al., 2010). Marais et al. (2016) applied an aqueous phase mechanism for SOA formation from isoprene in GEOS-Chem to reasonably simulate isoprene SOA in the southeast (SE) US. Accurate emission inventories are also needed to correctly represent volatile organic compounds (VOCs) and NO_x (NO_x = NO + NO_2) inputs, and these often have biases compared to observational constraints (Kaiser et al., 2018, Travis et al., 2016, Anderson et al., 2014; McDonald et al., 2018).

A quantitative measure of OA from space would be very helpful for verifying emissions and aerosol processes in models. However, direct measurements of OA from space are currently unavailable. Aerosol optical depth (AOD) measured by satellite sensors provides a coarse but global picture of total aerosol distributions. Multi-angle Imaging SpectroRadiometer (MISR) provides aerosol property information such as size, shape and absorbing properties, which allows retrieving AOD of a subset of aerosols (Kahn and Gaitley, 2015). Classification algorithms have been developed to speciate different aerosol types such as OA based on AOD, extinction Angstrom exponent, UV Aerosol Index, and trace gas columns from satellite instruments (de Vries et al., 2015).

Formaldehyde (HCHO) is one of the few VOCs that can be directly observed from space. Sources emitting POA (e.g., biomass burning (BB)) often simultaneously release VOCs. HCHO and SOA are also both produced from emitted VOCs. VOCs, as well as semi- and intermediate- volatile organic compounds (S/IVOCs), are oxidized by hydroxyl radicals (OH) to form peroxy radicals (RO_2), which then react with NO, RO_2, hydroperoxy radicals (HO_2) or isomerize. These oxidation processes produce HCHO and oxidized organic compounds with low volatility that condense to form SOA (Robinson et al., 2007; Ziemann and Atkinson, 2012). The yield of HCHO and SOA from hydrocarbon oxidation varies, depending on the VOC precursors, oxidants (OH, O_3 and NO_3), RO_2 reaction pathway (e.g. NO levels), and pre-existing aerosol abundance and properties (Wolfe et al., 2016; Pye et al., 2010; Marais et al., 2016 and 2017; Xu et al., 2016). Although the lifetime of HCHO (1-3 hrs) is shorter than OA (1 week), HCHO continues to form from slower reacting VOCs, as well as from the oxidation of later generation products. Observations across megacities around the world show that OA formation in polluted/urban area happens over about 1 day (e.g. DeCarlo et al., 2010; Hodzic and Jimenez, 2010; Hayes et al., 2013; 2015), and HCHO is also significantly formed over this timescale (Nault et al., 2018). Veefkind et al. (2011) found that satellite AOD correlated with HCHO over the summertime SE US, BB regions, and Southeast Asian industrialized regions. This also suggests that OA, a major contributor to AOD in the above cases (Jimenez et al., 2009), and HCHO share common emission sources and photochemical processes. Marais et al. (2016) further used the relationship between aircraft OA and satellite HCHO to evaluate GEOS-Chem representation of SOA mass yields from biogenic isoprene in the SE US.

We present an OA surface mass concentration estimate (OA estimate) derived from a combination of satellite HCHO column observations and in situ OA and HCHO relationships. The detection limit of satellite HCHO column observations limit the quality of OA estimate, thus we are focusing on summer time when HCHO levels are high. The OA estimate is evaluated against OA measurements at ground sites. A 3-D model GEOS-Chem OA simulation is also shown for comparison.

2. Methods

2.1 In situ airborne observations

Figure 1 shows flight tracks of field campaigns used in the current study. The Studies of Emissions, Atmospheric Composition, Clouds and Climate Coupling by Regional Surveys (SEAC^{4}RS) mission (Toon et al., 2016) covered the continental US with a focus on the SE US in August-September 2013. The Deep Convective Clouds & Chemistry Experiment (DC3) (Barth et al., 2015) surveyed the central and SE US in May-June 2012 while targeting isolated deep convective thunderstorms and mesoscale convective systems. The California Research at the Nexus of Air Quality and Climate Change (CalNex) (Ryerson et al., 2013) investigated the California region in May-June 2010, targeting the Los Angeles (LA) Basin and Central Valley. The Korea-United States Air Quality Study (KORUS-AQ) studied South Korean air quality, including sampling many large urban areas in South Korea and continental Asian outflow over the West Sea, in May-June 2016 (https://www-air.larc.nasa.gov/missions/korus-aq/). KORUS-AQ only includes data with longitude < 133° E to exclude the transit from US because it targeted

South Korea and the nearby region. These field campaigns were selected as they had recent high-quality in situ HCHO and OA data measured with state-of-the-art instruments and studied summertime regional tropospheric chemical composition.

In situ airborne HCHO observations were acquired by multiple instruments. The DC3 NASA DC-8 payloads featured two HCHO measurements: the NASA In Situ Airborne Formaldehyde (ISAF) (Cazorla et al., 2015) and the Difference Frequency Generation Absorption Spectrometer (DFGAS) (Weibring et al., 2006). The SEAC^{4}RS NASA DC-8 payloads also featured two HCHO measurements: the NASA ISAF and the Compact Atmospheric Multispecies Spectrometer (CAMS) (Richter et al., 2015). HCHO measurements from ISAF were found to be in good agreement with CAMS, with a correlation coefficient of 0.99 and a slope of 1.10 (Zhu et al., 2016). HCHO measurements from ISAF also had a good agreement with DFGAS, with a correlation coefficient of 0.98 and a slope of 1.07. Because ISAF has higher data density, we used ISAF HCHO data for DC3 and SEAC^{4}RS. During KORUS-AQ, CAMS was the only HCHO instrument onboard the DC-8. In CalNex a proton transfer reaction mass spectrometer (PTRMS) (Warneke et al., 2011) was used to measure HCHO on board the NOAA P3 aircraft.

In situ airborne OA from SEAC^{4}RS, DC3, and KORUS-AQ was measured by the University of Colorado High-Resolution Time-of-Flight Aerosol Mass Spectrometer (AMS, DeCarlo et al., 2006; Dunlea et al., 2009; Canagaratna et al., 2007; Jimenez et al., 2016) and in situ airborne OA from CalNex was measured by the NOAA Compact Time-

of-Flight Aerosol Mass Spectrometer (Drewnick et al., 2005; Canagaratna et al., 2007; Bahreini et al., 2012). The OA measurements are from 1 min merge data and converted from μg sm^{-3} (at 273 K and 1013 mbar) to μg m^{-3} under local T & P for each data point.

Although NO modulates the RO_2 lifetime, and thus, the production of HCHO and SOA, it cannot be directly observed via remote sensing. Instead, NO_2 can be directly observed in space by satellites, and since NO_2 represents typically ~80% (e.g. $SEAC^4RS$ and KORUS-AQ) of the boundary layer NO_x concentrations during the daytime, it can be used as a surrogate for daytime NO concentrations and oxidative conditions around the globe. In situ airborne NO_2 was measured by the NOAA Chemiluminescence NO_yO_3 instrument (Ryerson et al., 2001) during $SEAC^4RS$ and by University of Berkeley laser induced fluorescence NO_2 instrument (Day et al., 2002) during KORUS-AQ.

2.2 Ground-based OA measurements

Ground-based OA measurements over the US are from the EPA Interagency Monitoring of Protected Visual Environments (IMPROVE) (Malm et al., 1994; Solomon et al., 2014; Hand et al., 2014; Hand et al., 2013; Malm et al., 2017) and Southeastern Aerosol Research and Characterization (SEARCH) (Edgerton et al., 2006) networks. In the IMPROVE network, aerosols were collected on quartz fiber filters and analyzed in the lab by thermal optical reflectance for organic and elemental carbon. The data were reported every three days from 1988 to 2014. Monthly averages were used for comparison in this study. IMPROVE OA data over the SE US (east of 70ºW) in summertime were multiplied by a factor of 1.37 to correct for partial evaporation during

filter transport, following the recommendation of a comparison study with SEARCH organic carbon (OC) measurements (Kim et al., 2015; Hand et al., 2013). Although IMPROVE OA corrected for evaporation has potential uncertainties with the constant scaling factor, the IMPROVE measurements have high spatial coverage. SEARCH network (Edgerton et al., 2006; Hidy et al., 2014) OC is determined by the difference between total carbon (TC) detected by a tapered element oscillating microbalance (TEOM) and black carbon (BC) measured by an in situ Thermal Optical instrument. This allows real-time measurement of OC and prevents evaporation during filter transport. Although the SEARCH network only has 5 sites available, we also use observations from this network due to their high accuracy. The IMPROVE and SEARCH network OC measurements were converted to OA by multiplying by a factor of 2.1 based on ground and aircraft observations (Pye et al., 2017; Schroder et al., 2018).

2.3 Satellite measurements

Satellite HCHO column observations are derived from the NASA's Ozone Monitoring Instrument (OMI), a UV/Vis nadir solar backscatter spectrometer on the Aura satellite (Levelt et al., 2006). Aura overpasses the equator at 1:30 pm local time, daily. Here we use the OMI HCHO version 2.0 (collection 3) gridded (0.25°× 0.25°) retrieval data (Gonzalez Abad et al., 2015) from the Smithsonian Astrophysical Observatory (SAO). Satellite data for HCHO columns were subjected to data quality filters: 1) solar zenith angle lower than 70°, 2) cloud fraction less than 40%, and 3) main quality flag and the xtrackquality flag both equal to zero (https://www.cfa.harvard.edu/atmosphere/Instruments/OMI/PGEReleases/READMEs/O

MHCHO_README_v3.0.pdf). The monthly average HCHO columns were also weighted by the column uncertainties of the pixels. The HCHO retrieval used a priori profiles without aerosol information from the GEOS-Chem model (Gonzalez Abad et al., 2015). Satellite NO_2 column observations are also derived from NASA's OMI level 3 data, archived at hbps://disc.sci.gsfc.nasa.gov as "OMI-Aura_L3-OMNO2d" (Lamsal et al., 2014).

Satellite AOD observations were acquired from the Moderate Resolution Imaging Spectroradiometer (MODIS) onboard the Aqua satellite, using overpasses at about 1:30 pm local time. Here, we use collection 06 (MYD04_L2, hbps://ladsweb.nascom.nasa.gov/), retrieved using the Dark Target (DT) and Deep Blue (DB) algorithms (Levy et al., 2015).

2.4 GEOS-Chem

We used GEOS-Chem (v9-02) at 2° × 2.5° with 47 vertical layers to simulate HCHO and OA globally, the same as that in Marais et al. (2016). GEOS-Chem is driven with meteorological fields from the NASA Global Modeling and Assimilation Office (GMAO). The OA simulation includes POA from fires and anthropogenic activity and SOA from the volatility-based reversible partitioning scheme (VBS) of Pye et al. (2010) for anthropogenic, fire, and monoterpene sources, and an irreversible aqueous-phase reactive uptake mechanism for isoprene. The aqueous-phase mechanism is coupled to gas-phase isoprene chemistry and has been extensively validated using surface and aircraft observations of isoprene SOA components in the SE US (Marais et al., 2016).

This model version uses the fourth-generation global fire emissions database (GFED4) (Giglio et al., 2013) as BB emission inventory. The model is driven with Goddard Earth Observing System – Forward Processing (GEOS-FP) meteorology for 2013 and sampled along the SEAC^{4}RS (2013) and KORUS-AQ (2016) flight tracks. The model was also run with 10% decrease in biomass burning, biogenic, or anthropogenic emissions as sensitivity test to evaluate the contributions of different sources to OA and HCHO budget. Model monthly mean surface layer OA and total column formaldehyde are obtained around the OMI overpass time (12:00-15:00 local time) for 2008-2013 using MERRA Modern-Era Retrospective analysis for Research and Applications (MERRA) meteorology, as GEOS-FP is only available from 2012. This is compared to the OA estimate derived from satellite HCHO.

Global isoprene emissions are used to calculate an isoprene and NO_2 dependent OA estimate. Global isoprene emissions are from the Model of Emissions of Gases and Aerosols from Nature version 2.1 (Guenther et al., 2006) as implemented in GEOS-Chem and driven with MERRA (MEGAN-MERRA).

2.5 Estimation of surface organic aerosol mass concentrations

An estimate for surface OA mass concentration is calculated based on a simple linear transformation.

$$\varepsilon(\mathrm{i}) = \Omega_{HCHO}(\mathrm{i})\eta(\mathrm{i})\alpha(i) + \beta(\mathrm{i}) \qquad \text{Eq. (1)}$$

Here, ε(i) is the OA estimate for grid cell i (μg m^{-3}), Ω_{HCHO}(i) is the OMI HCHO column density (molec cm^{-2}) in each 0.25°×0.25° grid cell (similar resolution to OMI HCHO nadir pixel data), η(i) is the ratio of midday surface layer (~140 m) HCHO concentrations (molec cm^{-3}) to column concentrations (molec cm^{-2}) from GEOS-Chem, and $\alpha(i)$ and β(i) are the slope and intercept of a linear regression between OA and HCHO from low altitude (<1 km) airborne in situ measurements. The in situ to column conversion factor η(i) is similar to that used by Zhu et al. (2017) to convert HCHO columns into surface concentrations. η(i) is derived from the HCHO a priori profiles used in SAO OMI air mass factor (AMF) calculations (GEOS-Chem v9-01-03 climatology) or from GEOS-Chem v9-02, which includes updated isoprene scheme for OA and is the next version of the model (v9-01-03) for a priori profiles used in SAO satellite HCHO retrievals. HCHO a priori profiles are used to be consistent with satellite HCHO retrievals and also to show that OA estimate can be derived without running a global model separately. The newer version of GEOS-Chem is used to test the sensitivity of OA estimates to updated version of η. The newer version of GEOS-Chem also allows sampling through the flight tracks of a recent field campaign (SEAC^{4}RS) flight tracks and examining the factors impacting η with both modeled and measured HCHO profiles. The detailed information about the impact of HCHO profiles on η is provided in Sect. 5.

2.6 Aerosol extinction from satellite measurements

Currently remote sensing observes aerosols by quantifying AOD. The MISR satellite instrument can estimate a subset of AOD, due to constraints on size range, shape and absorbing properties, but cannot distinguish OA from other submicron aerosol

compounds such as sulfate and nitrate and also requires AOD above 0.1. Because MISR estimates a subset of AOD, it is discussed here to verify we are not neglecting a satellite dataset that has already captured OA AOD. Moreover, OA account for a large and relatively constant fraction of submicron aerosols in the SE US (Kim et al., 2015; Wagner et al., 2015) and is one of the major submicron aerosol components over the US (Jimenez et al., 2009). Therefore, AOD was converted to extinction to represent OA for comparison.

$$A_{ext} = \mathrm{AOD(i)}\delta\mathrm{(i)} \quad \text{Eq. (2)}$$

where A_{ext} is the calculated aerosol extinction (Mm^{-1}), AOD(i) is aerosol optical depth from MODIS (see Sect. 2.3) in each 0.25°×0.25° grid cell, and δ(i) (m^{-1}) is the ratio of surface layer OA concentrations ($\mu g\ m^{-3}$) to column OA concentrations ($\mu g\ m^{-2}$) from GEOS-Chem multiplied by 10^6 Mm^{-1}/m^{-1}. The shape of the average vertical profile of OA was very close to that of total aerosol mass over SE US (Wagner et al., 2015) where most of the enhanced aerosol concentrations over the US are located. Data with smoke plumes interferences are excluded in the following analysis. The potential contribution of dust and nitrate could alter the shape of the vertical profiles and introduce uncertainties when using OA vertical profiles for other parts of the US. Similar vertical profile shapes of OA and submicron particles were also observed in a campaign outside the US over South Korea (Nault et al., 2018). Though OA accounted for ~40% of the total submicron particles, the shape of OA and total submicron particles vertical profiles were nearly identical.

3. In situ OA and HCHO relationship

315 Although OA and HCHO share common VOC emission sources and photochemical
316 processes, their production rates from different emission sources and photochemical
317 conditions vary, as do their loss rates. The following section discusses the main factors
318 that modulate OA-HCHO relationships.
319
320 **3.1 Regional and Source-Driven Variability**
321 For all regions and/or sources investigated, near-surface in situ OA and HCHO are well
322 correlated. A scatter plot of in situ OA vs. HCHO at low altitudes (<1 km) from a number
323 of field campaigns (SEAC^{4}RS, DC3, CalNex, and KORUS-AQ) is displayed in Fig. 2.
324 The slope, intercept and correlation coefficient are provided in Table 1. SEAC^{4}RS, DC3,
325 and CalNex excluded BB data when acetonitrile > 200 pptv (Hudson et al., 2004).
326 KORUS-AQ used a BB filter with higher acetonitrile (>500 pptv) because the air masses
327 with moderate acetonitrile enhancement (200-500 pptv) were actually from
328 anthropogenic emissions. This attribution is based on high levels of acetonitrile detected
329 downwind of Seoul and west coastal petrochemical facilities, the slope between
330 acetonitrile and CO being to urban emissions (Warneke et al., 2006), and the
331 concentrations of anthropogenic tracer $CHCl_3$ being high (Warneke et al., 2006). Similar
332 to acetonitrile, another common BB tracer hydrogen cyanide (HCN) was also enhanced
333 in these air masses. BB data (acetonitrile > 200 pptv) for SEAC^{4}RS were analyzed
334 separately and are inset in Fig. 2. Although all CalNex data had a tight correlation, we
335 only included the flight data near LA basin to target the area strongly influenced by
336 anthropogenic emissions. In general, the correlation coefficients between in situ OA and
337 HCHO were strong (r = 0.59 –0.97) (Table 1).

The variety in OA-HCHO regression coefficients among different campaigns reflects the regional and/or source-driven OA-HCHO variability. Considering only the non-biomass burning (non-BB) air masses sampled, OA and HCHO had the tightest correlation for CalNex, because CalNex focused on the LA area (shown in Fig. 2) and Central Valley while SEAC^{4}RS and DC3 covered a larger area with a potentially larger variety of sources and chemical conditions. Although SEAC^{4}RS and DC3 both sampled the continental US, SEAC^{4}RS had more spatial coverage and sampled more air masses at low altitudes, while DC3 was designed to sample convective outflow air masses and had more data at high altitudes. Although KORUS-AQ covered a much smaller area compared to SEAC^{4}RS, KORUS-AQ data also had a large spread, which may be due to the complicated South Korean anthropogenic sources mixed with transported air masses (mainly from China) and possibly biogenic sources. OA exhibits a tight correlation with HCHO for both wildfires and agricultural fires during SEAC^{4}RS. This is because the production of HCHO and OA is much higher in BB air masses compared to background. This may also suggest that the emissions of OA and HCHO in these air masses are relatively constant. SEAC^{4}RS data are chosen because it sampled fires and had state-of-the-art, high quality measurements. More intensive fire sampling is needed to probe the correlation between OA and HCHO across fuel types and environmental conditions.

The different slopes of OA-HCHO among different campaigns also reflect the regional or source-driven OA-HCHO variability. The slopes of OA vs. HCHO were more similar between DC3 and SEAC^{4}RS. The slope of OA vs. HCHO was higher for South Korea (KORUS-AQ), which is dominated by anthropogenic emissions compared to the

362 biogenic-dominated emission in the SE US (SEAC^{4}RS and DC3). During KORUS-AQ,
363 the high OA/HCHO air masses also had high acetonitrile. By the time we sampled, most
364 organic aerosols were secondary (Nault et al., 2018). This indicates that the formation
365 rates of OA and HCHO from different emission sources contribute to the different slopes
366 of OA-HCHO. This also indicates that emission sources with enhanced acetonitrile tend
367 to form more OA relative to HCHO downwind. The slope of OA-HCHO for California
368 LA basin, dominated by anthropogenic emissions, was also not as high as South Korea.
369 The potential difference in the anthropogenic emissions mix could contribute to the
370 different OA-HCHO slopes from US LA region and South Korea anthropogenic sources
371 (Baker et al., 2007; Na et al., 2005; Na et al., 2002). The slopes of OA vs. HCHO for BB
372 air masses were higher than for anthropogenic and biogenic sources. This is consistent
373 with high POA emission in BB conditions (Heald et al., 2008; Lamarque et al., 2010;
374 Cubison et al., 2011), with low addition of mass due to SOA formation (Cubison et al.,
375 2011; Shrivastava et al., 2017). The slope of OA to HCHO was higher for wildfires than
376 agricultural fires during SEAC^{4}RS. This is consistent with more OA emitted in wildfires
377 than agricultural fires (Liu et al., 2017). The factors driving higher OA to HCHO with
378 wildfires are not clear and may be related to burning conditions and fuels. As SEAC^{4}RS
379 had the largest geographic coverage for low altitude data over US, the campaign average
380 slope of OA vs. HCHO was used to represent the US region in summer, except large
381 cities where CalNex LA Basin data were used.
382
383
384 **3.2 Dependence on NO_x and VOCs speciation**

385 Biogenic and anthropogenic VOCs are oxidized by atmospheric oxidants (e.g. OH as the
386 dominant oxidant) to form RO_2. HCHO is produced from the reactions of RO_2 with HO_2
387 or NO, with RO_2+NO typically producing more HCHO than $RO_2 + HO_2$ (e.g. Wolfe et
388 al., 2016). RO_2 can react with HO_2, NO, or isomerize to form oxidized organic
389 compounds with high molecular weight and low volatility, which condense on existing
390 particles to form SOA. The products of RO_2 + NO tend to fragment instead of
391 functionalize and often lead to higher volatility compounds (e.g. HCHO) and thus less
392 SOA formation compared to the products of $RO_2 + HO_2$ (Kroll et al., 2006; Worton et al.,
393 2013). Therefore, with the same VOC, we expect more HCHO and less OA formed at
394 high NO conditions and vice versa. As mentioned before, NO_2 instead of NO is easily
395 measured from space and NO_2 typically is ~80% of NO_x in the boundary layer during the
396 day. Therefore, NO_2 is used as a surrogate for the NO levels influencing OA and HCHO
397 production. The yields of HCHO and SOA also depend on VOC speciation (e.g. Lee et
398 al., 2006). Specifically, isoprene has a higher yield of HCHO than most non-alkene
399 VOCs (Dufour et al., 2009).
400
401 A scatter plot of OA vs. HCHO for SEAC^{4}RS low altitude data is shown in Fig. 3(a). The
402 data are color-coded by the product of in-situ isoprene and NO_2, attempting to capture
403 time periods strongly influenced by oxidation products of isoprene at high NO
404 conditions. No obvious trends are evident when the data are instead color coded by NO_2
405 or isoprene only. This may be because isoprene (biogenic source) and NO_2
406 (anthropogenic sources) are generally not co-located in the US (Yu et al., 2016) and
407 isoprene is the dominant source of HCHO compared to anthropogenic VOCs in the US

408 (e.g. Millet et al., 2008). This plot shows that, at high NO_2 and high isoprene conditions,
409 less OA was formed for each HCHO produced generally. The correlation coefficient of
410 0.45 for high NO_2 and isoprene conditions during SEAC^{4}RS is not very high but still
411 shows significant dependence of the OA-HCHO relationship on the product of NO_2 and
412 isoprene, considering that these are ambient data and other factors (e.g. different specific
413 sources) also play a role in determining OA-HCHO relationships. This is consistent with
414 high NO and isoprene conditions promote HCHO formation over SOA formation. We
415 also looked at the dependence on peroxy acetyl nitrate (PAN), as PAN is a product of the
416 photo oxidation of VOCs, including isoprene, in the presence of NO_2. The dependence on
417 PAN was not as clear as on the product of NO_2 and isoprene.
418
419 KORUS-AQ OA vs. HCHO, color-coded with NO_2, is plotted in Fig. 3(b). The OA /
420 HCHO ratio clearly decreased as NO_2 levels increased during KORUS-AQ, suggesting
421 that high NO conditions accelerated HCHO formation more than they did SOA
422 production. OA-HCHO relationships do not have dependence on local time of the day
423 (not shown). This further confirms that NO_x is an important factor that affects the
424 OA/HCHO relationship. Compared to SEAC^{4}RS, the KORUS-AQ OA/HCHO ratio does
425 not depend on VOCs. This may be consistent with the dominant VOC being
426 anthropogenic VOCs that are co-located with NO sources. This may also suggest the
427 anthropogenic VOCs generally have a lower HCHO yield than does isoprene. Because
428 OA and HCHO were tightly correlated during CalNex and DC3, we did not parse for
429 NO_x. The NO_x range during DC3 low altitude data was smaller than KORUS-AQ and
430 SEAC^{4}RS. DC3 OA and HCHO relationships only had a slight dependence on NO_2 (not

shown here), largely due to the limited dataset. The NO_x range during CalNex low altitude data was large. The tight OA and HCHO correlation during CalNex could be due to the combination of different VOCs sources and NO_x levels.

4. Comparison of OA and HCHO relationship: in-situ vs. GEOS-Chem

In situ OA vs. HCHO relationships from SEAC^{4}RS low altitude non-BB (Fig. 4a), KORUS-AQ low altitude (Fig. 4b), and SEAC^{4}RS BB (Fig. 4c) air masses were compared to GEOS-Chem model simulations (Fig. 4d-4f) sampling along the corresponding flight tracks. Similar to the in situ data, GEOS-Chem model simulations also found correlations between OA and HCHO for these three regions, especially for SEAC^{4}RS non-BB. GEOS-Chem was intensively validated with in situ measurements for SE US (e.g. Marais et al., 2016; Kim et al., 2015). The ratios of the slopes between OA and HCHO for the US (SEAC^{4}RS), South Korea (KORUS-AQ), and wildfire cases (SEAC^{4}RS) from GEOS-Chem were 1:1.1:0.4, which was different from the in situ measurements ratios of 1:1.4:13 (Table 1). GEOS-Chem could not capture any wild fires in US during SEAC^{4}RS, which is probably due to poor representation of BB emission inventory for US wildfire and also the coarse grid in GEOS-Chem. GEOS-Chem also significantly under predicted the slope of OA to HCHO for South Korea. We attribute this to a likely underprediction of anthropogenic SOA, which was dominant in South Korea, in GEOS-Chem (Schroder et al., 2018), as well as a different mix of OA and HCHO sources in the US compared to South Korea and representation of these in GEOS-Chem. Although GEOS-Chem contains isoprene chemistry with a focus on the SE US

(Marais et al. 2016), there is still room to improve the model especially for anthropogenic and BB sources, as well as anthropogenic OA formation mechanisms. For example, in the model biogenic sources are more important than anthropogenic sources for the OA and HCHO budgets in South Korea, which is not the case from KORUS-AQ in situ measurements. In the model, a 10% decrease of emissions from biogenic, anthropogenic and BB sources results in a 6%, 3%, and 1% decrease in OA and 2%, 1%, and 0% decrease in HCHO over South Korea in May 2016. However, the in situ airborne field campaign KORUS-AQ found that OA and HCHO were higher near anthropogenic emission sources compared to rural regions. The larger impact of biogenic sources compared to anthropogenic sources on OA and HCHO in the model can be due to both low-biased anthropogenic emission inventories and low-biased anthropogenic SOA. Improving anthropogenic emissions inventories in the models can also bring model results closer to observations. Improving anthropogenic SOA, such as implementation of the SIMPLE model, in GEOS-Chem (Hodzic and Jimenez, 2011) can also improve the model results compared to observations. Measurements or measurement-constrained estimation with sufficient spatial and temporal coverage can help to narrow down the key factors (e.g. emission inventories or chemical schemes) in GEOS-Chem to better represent VOCs and OA globally. Furthermore, we did also find that GEOS-Chem could not capture the observed higher slope of OA to HCHO at high altitudes (not shown), which could be due to issues such as transport, OA lifetime, and OA production.

5. Relating satellite HCHO column to surface HCHO concentrations

To utilize the derived in-situ OA and HCHO relationship, the satellite HCHO column needs to be converted to surface HCHO concentrations. We used a vertical distribution factor η (cm^{-1}) (Sect. 2.5), which is defined as the ratio of surface HCHO concentrations (molec cm^{-3}) to HCHO column (molec cm^{-2}), to estimate surface HCHO concentrations from satellite column measurements. Zhu et al. (2017) used the same vertical distribution factor for their study. The use of this factor is justified by the fact that the derived surface HCHO retained the spatial pattern of the satellite HCHO column and agreed with local surface measurements of HCHO for a multi-year average (Zhu et al., 2017).

We also investigated the main factors affecting the variation of the vertical distribution factor η. Because the factor is determined by HCHO vertical distributions, we examined three typical normalized HCHO vertical distribution profiles with the highest, median and lowest η values for the SEAC^{4}RS field campaign (Fig. 5). Because the sensitivity of OA estimates to η is investigated with η from different GEOS-Chem versions (Sect. 6.2), we don't compare HCHO vertical profiles from model and measurements for a comprehensive set of field campaigns. We chose SEAC^{4}RS to illustrate the main factors impacting the η over US because SEAC^{4}RS has a larger spatial coverage than DC3 and CalNex. GEOS-Chem can generally capture the vertical profiles of measured HCHO. Boundary layer mixing height and surface emission strength are the dominant factors in determining the fraction of HCHO near the surface. We can see that higher boundary layer mixing height results in lower η for SE US profiles, where there are biogenic sources of HCHO from the surface and HCHO has distinct concentration difference

below and above the boundary layer. However, there are exceptions, such as for the profiles over the ocean and the coastal regions. Although the boundary layer is shallow in these regions, a large portion of HCHO resides above the boundary layer, resulting in low η. In these cases, surface emissions of HCHO or precursors are very small and therefore methane oxidation makes a large contribution to the total HCHO column. High concentrations of HCHO (e.g., in BB plumes) lofted by convection can also impact the vertical profile (Barth et al., 2015), which is not further investigated because OA estimates with BB influences over US are excluded in current study. Overall, the source intensities and boundary layer mixing height mostly determined the HCHO vertical profiles.

6. Construction of the OA estimate

6.1 Variables to construct OA estimate

As mentioned in Sect. 2.5, the OA estimate value in each grid cell is estimated from monthly average satellite HCHO column observation by the linear Eq. (1). Satellite monthly average HCHO column data, Ω_{HCHO}, are converted to surface HCHO concentrations by multiplying by the η(i) factor either from climatology a priori profiles or monthly average HCHO profiles. Surface OA is then estimated by the derived surface HCHO concentrations and applying the linear regression equation (slope $\alpha(i)$ and intercept β(i)) between in situ OA and HCHO determined from in-situ aircraft field campaign data. The relationship between OA and HCHO varies but previous sections demonstrated that we can quantify the surface OA-HCHO relationship by their regions, sources and chemical conditions (e.g., NO_x levels). To test the impact of the chosen OA-

523 HCHO relationship on the calculated OA estimate, the OA estimate in the US was
524 calculated using four different methods (see Table 2).
525
526 **6.2 OA estimate over US**
527 The monthly average surface OA estimate over the US in August 2013 for case 1 (see
528 Table 2) with different η is shown in Fig. 6a and 6b. Because BB regions in the US are
529 not covered by smoke continuously during a period of time and it is challenging for
530 satellite retrieval to separate thick BB plumes and clouds without information on the time
531 and location of the burning, thick BB events (OMI UV Aerosol Index (UVAI) > 1.6)
532 (Torres et al., 2007) were excluded and shown as the blank (white) grid cells in Fig. 6a
533 and 6b. The same filter was also applied to aerosol extinction and GEOS-Chem OA
534 abundance. To evaluate the representative quality of the OA estimate, OA estimate data
535 were compared to the EPA IMPROVE ground sites corrected-OA measurements over the
536 US and SEARCH ground sites OA measurements in the SE US (Sect. 2.2). The locations
537 of IMPROVE and SEARCH sites are displayed in Fig. 6e as small and large dots,
538 respectively. The dot color represents the average OA mass concentrations for August
539 2013.
540
541 Considering the uncertainties in satellite HCHO measurements, in using the campaign
542 lump-sum OA-HCHO relationship to represent spatial resolved OA, in HCHO vertical
543 profiles, and in ground IMPROVE network measurements, the correlation (correlation
544 coefficient r = 0.56) between the OA estimate and corrected IMPROVE network
545 measurements (Fig. 6f and 6g) is reasonably good and indicates that the OA estimate can

546 generally capture the variation of OA loading over the US. The correlation coefficient
547 between HCHO SAO retrievals and in situ measurements during SEAC^{4}RS was not
548 high (r = 0.24) but this may be partly because they were not sampled at the same time.
549 The uncertainty in HCHO SAO data was likely less than 76%. The uncertainty in
550 applying a campaign lump-sum OA-HCHO relationship to individual spatial resolved
551 satellite HCHO data to estimate OA induced an uncertainty of 41% according to the
552 correlation coefficient of OA-HCHO in the field campaign. η in the Fig. 6a OA estimate
553 is from GEOS-Chem v9-02 output for the specific month August, 2013. η in the Fig. 6b
554 OA estimate is from GEOS-Chem v9-01-03 climatology, the same as satellite data a
555 priori profiles. The good correlations of OA estimates with IMPROVE OA indicate that
556 OA estimates are not very sensitive to η from different model versions. The largest
557 difference between the two OA estimates is their concentrations over East Texas. There
558 are no IMPROVE OA measurements in the East Texas to evaluate which works better.
559 The uncertainties in IMPROVE OA measurements, such as using a constant correction
560 factor to correct the partial evaporation across all SE US sites, and the spatially
561 dependent OA/OC ratio (Tsigaridis et al., 2014), may also have contributed to the
562 discrepancies between the OA estimate and EPA IMPROVE sites OA. Therefore, higher
563 quality of satellite HCHO data and refining OA-HCHO relationships will help improve
564 our OA estimate products. This combined with a spatially resolved IMPROVE OA
565 correction factor and OA/OC ratios will help improve the correlation coefficients
566 between OA estimates and IMPROVE OA.
567

568 The linear correlation between the OA estimate and IMPROVE OA measurements
569 yielded a slope of 0.62 or 0.60, indicating that the OA estimate slightly underestimated
570 OA. Satellite HCHO data were measured in mid-day, in situ airborne OA and HCHO
571 were measured during the daytime and IMPROVE network organic carbon was collected
572 day and night. Because ground OA in the SE US were observed to have little diurnal
573 variation (Xu et al., 2015; Hu et al., 2015), the different sampling time of ground and
574 airborne OA probably does not have a significant impact on the comparison of OA
575 estimate and IMPROVE OA. Surface HCHO has evident diurnal profiles with the highest
576 concentrations around the mid-day (Kaiser et al., 2016), which could add uncertainties to
577 OA estimate when using inconsistent time ranges of satellite HCHO data measured in the
578 mid-day and in situ airborne OA and HCHO relationships measured in the daytime. The
579 SEAC^{4}RS HCHO concentrations were converted to 1:30 pm concentrations according to
580 the average HCHO diurnal profile from the Southern Oxidant and Aerosol Study (SOAS)
581 (Kaiser et al., 2016). The OA-HCHO relationship with HCHO converted to 1:30 pm
582 yielded a slope of 5% lower than the original OA-HCHO relationship. The potential
583 uncertainty ($\pm$30%) in OA/OC ratio could also contribute to the systematic difference
584 because we used OA/OC of 2.1 and studies (e.g. Pye et al., 2017; Canagaratna et al.,
585 2015) showed that the OA/OC can range from 1.4 to 2.8. The potential underestimation
586 of HCHO from satellite retrieval (by –37%) (Zhu et al., 2016) compared to SEAC^{4}RS
587 may be one of the most important reasons that cause the systematic difference (low slope)
588 between the OA estimate and IMPROVE OA according to Eq. (1). Satellite HCHO data
589 corrected by the low bias (by –37%) (Zhu et al., 2016) will increase our slopes of 0.60-
590 0.62 to be close to the unity.

SEARCH OA data were also used to compare to the OA estimate. The correlation was good for August 2013. Although the SEARCH network OA measurements have better accuracy, the number of SEARCH sites is limited (5 sites). The correlation of OA estimate and SEARCH OA varied dramatically 2008-2013 (Fig. S1). GEOS-Chem OA does not correlate with SEARCH OA except for the year 2013 (Fig. S1). As the IMPROVE network has more sites and spatial coverage, we use IMPROVE network data as ground OA measurements for comparison in the remainder of the discussion.

6.3 Comparison to aerosol extinction from AOD

To further evaluate the method of using satellite HCHO to derive an OA surface estimate, satellite aerosol measurements are used to approximate surface OA extinction for comparison. Satellite measurements of AOD were converted to surface extinction for the regions AOD is dominated by OA (see Sec. 2.6). Studies showed that OA were a dominant component of aerosol mass and extinction during SEAC^{4}RS (Kim et al., 2015; Wagner et al., 2015) and the fractions of OA were relatively constant (interdecile 62-74%) (Wagner et al., 2015). Therefore AOD variation is expected to generally reflect the OA variation during SEAC^{4}RS. Satellite measurements from MISR can provide more aerosol property information to apportion total AOD to AOD of a subset of aerosols with small to medium size and round shape, which can better capture OA, when AOD is above 0.15 to 0.2 (Kahn and Gaitley, 2015; personal communication with R. Kahn, 2018). Because MISR cannot distinguish OA and other submicron aerosol components (e.g. sulfate and nitrate) and would cut off low AOD data which accounted for near half of the

614 data over US, we use total AOD to derive extinction for our comparison. The AOD-
615 derived extinction map is shown in Fig. 6(c), and the scatter plot of AOD-derived
616 extinction and EPA corrected OA is displayed in Fig. 6(h). The same filter of high AI
617 was also applied to AOD-derived extinction to remove BB plumes. Generally, the
618 derived aerosol extinction had a correlation with IMPROVE OA, but the correlation is
619 not as good as for the OA estimate with IMPROVE OA. The high surface aerosol
620 extinctions (> 150 Mm^{-1}) (outliners in the scatter plot) are located in the SE US and
621 therefore are not due to potential contribution of dust and nitrate altering the shape of
622 vertical profiles outside of the SE US. This indicates that the OA estimate derived from
623 HCHO may be better than AOD at representing the concentrations of OA, even for the
624 regions where AOD is dominated by OA (Xu et al., 2015).
625
626 **6.4 Comparison to GEOS-Chem OA**
627 Surface OA over the US from a GEOS-Chem simulation for August 2013 is shown in
628 Fig. 6(d), and the scatter plot of GEOS-Chem OA with IMPROVE OA is in Fig. 6(i). The
629 GEOS-Chem simulation had a coarser resolution than satellite HCHO data. To be
630 comparable to the OA estimate, the scatter plot Fig. 6(i) used GEOS-Chem results for the
631 grid squares that overlap with individual IMPROVE sites. Compared to the OA estimate,
632 GEOS-Chem OA had a similar correlation coefficient with IMPROVE OA. Although the
633 GEOS-Chem OA plot appears more scattered, there are many GEOS-Chem data points
634 close to zero when IMPROVE OA was low, making the overall correlation coefficient
635 similar to that for the OA estimate. GEOS-Chem under predicted IMPROVE OA more

636 with a slope of 0.57 compared to the OA estimate. This is consistent with underprediction
637 of anthropogenic OA in Marais et al. (2016).
638
639 **6.5 OA estimate with different OA-HCHO relationships**
640 In general, OA estimate results from the four cases were similar. The OA estimates from
641 the four cases (Table 2) were compared to IMPROVE OA and the correlation coefficients
642 are shown in Fig. 7. The details about how to implement chemical factors dependent OA
643 estimates for the four cases are also provided in Table 2. Satellite OMI NO_2 data (at 1 :
644 30 pm) are used to represent NO_x levels, big cities are defined as $NO_2 > 4 \times 10^{15}$ molec
645 cm^{-2} and the CalNex in situ OA-HCHO relationship is applied for big cities. It turns out
646 that only 1 IMPROVE site (San Gabriel, SAGA1) near LA was affected by high NO_2 and
647 led to the insignificant change in case 3 compared to case 1. This is not unexpected
648 because IMPROVE sites are in rural regions. The OA estimate in SAGA1 decreased from
649 1.88 $\mu g\ m^{-3}$ from case 1 to 0.17 $\mu g\ m^{-3}$ in case 3 while the measured OA in IMPROVE
650 SAGA1 was 1.52 $\mu g\ m^{-3}$. This may infer that CalNex is not very consistent with
651 SEAC^{4}RS due to different sampling instruments, strategies and seasons. Lowing the NO_2
652 threshold when defining big cities did not help improve the agreement either. Including
653 the NO_2–isoprene-dependent OA and HCHO relationship (case 2) showed a similar (or
654 slightly worse) correlation between the OA estimate and IMPROVE OA. As the in situ
655 data showed a moderate NO_2–isoprene-dependent OA and HCHO relationship, we
656 attributed this to the uncertainty of isoprene emissions from MEGAN, the locations of
657 IMPROVE site at rural regions, the uncertainty in IMPROVE network measurements, or
658 other factors (e.g. sources-dependent OA-HCHO) besides NO_2-isoprene that also need to

659 be taken into account when determining the specific OA-HCHO relationship. Because
660 separating large urban areas and other regions and applying a simple chemical regime
661 dependent in situ OA and HCHO relationship did not improve the agreement between the
662 OA estimate and IMPROVE OA, we used the base case OA and HCHO relationship
663 (case 1) to derive the OA estimate (shown in Fig. 6). SEAC^{4}RS and DC3 only had a few
664 low altitude data in the Midwest and did not cover the Northeast US. The measured OA-
665 HCHO relationship in the Midwest did not show significant difference from the SE US.
666 The scatter plots (Fig. 6f and 6g) of OA estimates and IMPROVE OA do not show
667 outliners for the Northeast and Midwest. This indicates that using the SEAC^{4}RS lump
668 sum OA-HCHO relationship can reasonably capture regions outside of the SE US.
669
670
671 **6.6 Temporal variation of the agreement between OA estimate and IMPROVE OA**
672 Besides August 2013 (see Fig. 6), the correlations between the OA estimate and
673 IMPROVE OA for the summer months June-July-August 2008-2013 were also examined
674 and shown in Fig. 7. Generally, the correlation coefficients between the OA estimate and
675 IMPROVE OA were >0.5 for summer months of the years investigated. The correlation
676 coefficients were generally higher in June compared to July and August. The lower
677 average temperature in June might be related to the higher correlation coefficients.
678 IMPROVE network aerosol samples were transported at ambient temperature in a truck
679 and more organic vapors likely evaporated at higher temperature. The different
680 temperatures and distances from IMPROVE sites to the laboratory may lead to
681 inhomogeneous evaporation among the samples and result in lower correlation

coefficients. Although higher temperatures in July and August may also lead to more BB, average aerosol index over the US was not higher in July (mean: 0.35) and August (mean: 0.36) compared to June (mean: 0.39) for these years. The underlying cause for the lowest correlation coefficients in July and August 2012 is not clear and may be related the severe drought in 2012 (Seco et al., 2015). The correlation coefficients were also low for the linear regressions (not shown) of IMPROVE OA with both GEOS-Chem OA and AOD-derived extinction. Because the lowest correlation coefficients were consistently observed for multiple OA-related products and not just the OA estimate, we attributed this to uncertainties in the IMPROVE OA measurements or some unknown bias shared by the satellite HCHO, GEOS-Chem OA, and satellite AOD.

6.7 South Korea OA estimate

We attempted to estimate an OA estimate for South Korea, using airborne in situ measurements of OA and HCHO from the KORUS-AQ field campaign (https://www-air.larc.nasa.gov/missions/korus-aq/) and SAO OMI HCHO measurements. The National Institute of Environmental Research (NIER) ground sites OC measurements during KORUS-AQ over South Korea could be used to validate the OA estimate. However, OMI HCHO measurements were below the detection limit (Zhu et al., 2016) in May 2016. Also, there were no OMI data available in June 2016 when airborne measurements and ground sites OC measurements were available during KORUS-AQ. Because an OA estimate for South Korea could not be well retrieved and validated, it was not presented in this study. Although an OA estimate for South Korea could not be retrieved in the current study, the consistency in the dependence of OA-HCHO relationships on chemical

706 factors (e.g. emission sources, NO_x, and altitudes) provides important information for
707 potential application of chemical factors dependent OA-HCHO relationships to the
708 geographical domain beyond the continental US, especially with improved satellite
709 HCHO data from Tropospheric Monitoring Instrument (TROPOMI).
710
711 **7 Limitations of the OA estimate and future work**
712 Because the OA estimate is based on satellite HCHO data, the detection limit of satellite
713 HCHO data affects the quality of the OA estimate. Currently, due to the limited
714 sensitivity of OMI for HCHO, the OA estimate is valid only when high levels of HCHO
715 are present, such as during summer time and near large HCHO sources. With the new
716 TROPOMI satellite instrument and future missions TEMPO and GEMS, satellite HCHO
717 measurements will have higher spatial and temporal resolutions and lower detection
718 limits. These higher quality satellite HCHO measurements will improve our OA estimate
719 quality and also its spatial and temporal coverage.
720
721 Because the OA estimate uses the relationship of in situ HCHO and OA measurements,
722 the coverage of in situ aircraft field campaigns will impact the OA estimate quality.
723 Currently, in situ airborne measurements of OA and HCHO focus on the continental US.
724 Extending measurements to regions such as Africa BB, South America, and East Asia,
725 where HCHO and OA have high concentrations, will increase the spatial coverage of the
726 OA estimate product. Ground site measurements of OA with consistent quality control in
727 those regions will also be important for validating the OA estimate.
728

729 Improvement of satellite HCHO retrieval during the BB cases will also improve OA
730 estimate quality. BB cases with high UV aerosol index over the US were excluded in the
731 current OA estimate analysis. With improvement in the satellite retrieval of HCHO, we
732 may be able to estimate OA during BB cases over the US. Upcoming field campaigns
733 such as the Fire Influence on Regional and Global Environments Experiment – Air
734 Quality (FIREX-AQ) will provide opportunities to improve the analysis of OA estimate
735 in BB cases in the US.
736
737 This OA estimate method has limitations in remote regions far away from HCHO
738 sources. Because the lifetimes of HCHO (1-3 hours) and OA (1 week) are different, the
739 slopes and intercepts between HCHO and OA are expected to change when air masses
740 are aged (e.g. in remote regions). HCHO is close to being in steady-state with production
741 rates roughly equal to loss rates while OA is not in steady-state with a lifetime of a week.
742 Therefore, OA can be accumulated relative to HCHO when air masses are aged. OA vs.
743 HCHO from SEAC^{4}RS and KORUS-AQ field campaigns, color-coded with altitude as an
744 indicator of air mass age, are plotted in Fig. S2 (a) and (b), respectively. A relative
745 depletion of HCHO at high altitudes was observed due to its shorter lifetime. This also
746 suggests that, at remote regions far away from the sources, the ratios of OA and HCHO
747 could be much higher and the relationship between OA and HCHO derived near the
748 sources may no longer apply. On the other hand, the lifetime of 1-3 hrs for HCHO does
749 not imply that the OA estimate only work within this timescale. HCHO is formed from
750 oxidation of transported gas phase VOCs, including the oxidation products of the primary
751 emitted VOCs, as well as of the slower reacting VOCs (e.g. Ethane and Benzene). Most

752 gas-to-particle oxidation processes that might produce HCHO can last up to 1-2 days
753 (Palm et al., 2018). Fig. S3 shows the ratios of OA and HCHO did not change
754 significantly downwind for the Rim Fire plume for about 1 day of aging, which was
755 determined by the distance from the source and the wind speed. A lower photolysis rate
756 of HCHO in the plume can also contribute to this. However, we do not expect that the
757 relationship of OA and HCHO remains past 1-2 boundary layer ventilation cycles (Palm
758 et al., 2018). Although OA-HCHO relationships depend on air mass age, it does not
759 largely affect our study for monthly average surface OA over continental US because our
760 OA estimates showed reasonably good agreement with ground sites IMPROVE OA
761 measurements. This also indicates that SOA are enhanced near the source regions
762 statistically. Nault et al. (2018) also showed the production of HCHO and SOA are
763 similar and plateau around 0.5 – 1 photochemical day. So, in the near field of emissions
764 and chemistry, the productions of these two species are similar; however, outside of near
765 field of emissions and rapid chemistry, the long lifetime of OA vs the steady state of
766 HCHO would start controlling the slopes and correlations.
767
768
769 **8 Summary**
770 We have developed a satellite-based estimate of the surface OA concentration ("OA
771 estimate") based on in situ observations. This estimate is based on the empirical
772 relationships of in-situ OA and HCHO for several regions. OA and HCHO share VOC
773 sources with different yields and lifetimes. Using surface OA and HCHO linear
774 regression slopes and intercepts can relate surface HCHO to OA. To estimate the surface

775 HCHO concentration from satellite HCHO column, we used a vertical distribution factor
776 η from either climatology satellite data a priori profiles or updated model run for specific
777 period, which is largely determined by boundary layer height and surface emissions and
778 found to reasonably retrieve surface HCHO from column HCHO.
779
780 The OA estimate over the continental US generally correlated well with EPA IMPROVE
781 network OA measurements corrected for partial evaporation. The good correlations are
782 not only for the time during SEAC^{4}RS but also for most summer months over several
783 years (2008-2013) investigated. Compared to aerosol extinction derived from AOD, the
784 OA estimate had slightly higher correlation coefficients with IMPROVE OA. GEOS-
785 Chem can predict OA with a similar correlation coefficient with IMPROVE OA
786 compared to the OA estimate when GEOS-Chem was intensively validated with in situ
787 measurements for SE US. Better satellite HCHO data from TROPOMI and future
788 TEMPO and GEMS and extending spatiotemporal coverage of in situ measurements will
789 improve the quality and coverage of the OA estimate.
790
791
792
793
794
795
796
797

Acknowledgements:

JL, TFH, GMW, and JSC were supported by NASA grant NNH15ZDA001N and NNH10ZDA001N. BAN, PCJ, and JLJ were supported by NASA grant NNX15AT96G and 80NSSC18K0630. AW and PTR-MS measurements during DC3, SEAC^{4}RS and KORUS-AQ were supported by the Austrian Federal Ministry for Transport, Innovation and Technology (bmvit) through the Austrian Space Applications Programme (ASAP) of the Austrian Research Promotion Agency (FFG). The PTR-MS instrument team (P. Eichler, L. Kaser, T. Mikoviny, M. Müller) is acknowledged for their field support. We thank E. Edgerton for providing the SEARCH network data.

811 References:

812 Anderson, D. C., Loughner, C. P., Diskin, G., Weinheimer, A., Canty, T. P., Salawitch, R. J.,
813 Worden, H. M., Fried, A., Mikoviny, T., Wisthaler, A., and Dickerson, R. R.: Measured and
814 modeled CO and NOy in DISCOVER-AQ: An evaluation of emissions and chemistry over the
815 eastern US, Atmos Environ, 96, 78-87, 10.1016/j.atmosenv.2014.07.004, 2014.
816
817 Attwood, A. R., Washenfelder, R. A., Brock, C. A., Hu, W., Baumann, K., Campuzano-Jost, P.,
818 Day, D. A., Edgerton, E. S., Murphy, D. M., Palm, B. B., McComiskey, A., Wagner, N. L., de
819 Sa, S. S., Ortega, A., Martin, S. T., Jimenez, J. L., and Brown, S. S.: Trends in sulfate and
820 organic aerosol mass in the Southeast U.S.: Impact on aerosol optical depth and radiative
821 forcing, Geophys Res Lett, 41, 7701-7709, 10.1002/2014gl061669, 2014.
822
823 Bahreini, R., Middlebrook, A. M., de Gouw, J. A., Warneke, C., Trainer, M., Brock, C. A., Stark,
824 H., Brown, S. S., Dube, W. P., Gilman, J. B., Hall, K., Holloway, J. S., Kuster, W. C., Perring,
825 A. E., Prevot, A. S. H., Schwarz, J. P., Spackman, J. R., Szidat, S., Wagner, N. L., Weber, R. J.,
826 Zotter, P., and Parrish, D. D.: Gasoline emissions dominate over diesel in formation of secondary
827 organic aerosol mass, Geophys Res Lett, 39, Artn L06805
828 10.1029/2011gl050718, 2012.
829
830 Baker, A. K., Beyersdorf, A. J., Doezema, L. A., Katzenstein, A., Meinardi, S., Simpson, I. J.,
831 Blake, D. R., and Rowland, F. S.: Measurements of nonmethane hydrocarbons in 28 United
832 States cities, Atmos Environ, 42, 170-182, 10.1016/j.atmosenv.2007.09.007, 2008.
833
834 Barth, M. C., Cantrell, C. A., Brune, W. H., Rutledge, S. A., Crawford, J. H., Huntrieser, H.,
835 Carey, L. D., MacGorman, D., Weisman, M., Pickering, K. E., Bruning, E., Anderson, B., Apel,
836 E., Biggerstaff, M., Campos, T., Campuzano-Jost, P., Cohen, R., Crounse, J., Day, D. A., Diskin,
837 G., Flocke, F., Fried, A., Garland, C., Heikes, B., Honomichl, S., Hornbrook, R., Huey, L. G.,
838 Jimenez, J. L., Lang, T., Lichtenstern, M., Mikoviny, T., Nault, B., O'Sullivan, D., Pan, L. L.,
839 Peischl, J., Pollack, I., Richter, D., Riemer, D., Ryerson, T., Schlager, H., St Clair, J., Walega, J.,
840 Weibring, P., Weinheimer, A., Wennberg, P., Wisthaler, A., Wooldridge, P. J., and Ziegler, C.:
841 The Deep Convective Clouds and Chemistry (Dc3) Field Campaign, B Am Meteorol Soc, 96,
842 1281-1309, 10.1175/Bams-D-13-00290.1, 2015.
843
844 Bianchi, F., Barmet, P., Stirnweis, L. El Haddad, I., Platt, S.M., Saurer, M., Lötscher, C.,
845 Siegwolf, R., Bigi, A., Hoyle, C.R., DeCarlo, P.F., Slowik, J.G., Prévôt, A.S.H., Baltensperger,
846 U., and Dommen. Contribution of methane to aerosol carbon mass. Atmospheric Environment,
847 141, 41-47, doi: 10.1016/j.atmosenv.2016.06.036, 2016.
848
849 Canagaratna, M. R., Jayne, J. T., Jimenez, J. L., Allan, J. D., Alfarra, M. R., Zhang, Q., Onasch,
850 T. B., Drewnick, F., Coe, H., Middlebrook, A., Delia, A., Williams, L. R., Trimborn, A. M.,
851 Northway, M. J., DeCarlo, P. F., Kolb, C. E., Davidovits, P., and Worsnop, D. R.: Chemical and
852 microphysical characterization of ambient aerosols with the aerodyne aerosol mass spectrometer,
853 Mass Spectrom Rev, 26, 185-222, 10.1002/mas.20115, 2007.
854
855 Canagaratna, M. R., Jimenez, J. L., Kroll, J. H., Chen, Q., Kessler, S. H., Massoli, P.,

Hildebrandt Ruiz, L., Fortner, E., Williams, L. R., Wilson, K. R., Surratt, J. D., Donahue, N. M., Jayne, J. T., and Worsnop, D. R.: Elemental ratio measurements of organic compounds using aerosol mass spectrometry: characterization, improved calibration, and implications, Atmos Chem Phys, 15, 253-272, https://doi.org/10.5194/acp-15-253-2015, 2015.

Carslaw, K. S., Lee, L. A., Reddington, C. L., Pringle, K. J., Rap, A., Forster, P. M., Mann, G. W., Spracklen, D. V., Woodhouse, M. T., Regayre, L. A., and Pierce, J. R.: Large contribution of natural aerosols to uncertainty in indirect forcing, Nature, 503, 67-+, 10.1038/nature12674, 2013.

Cazorla, M., Wolfe, G. M., Bailey, S. A., Swanson, A. K., Arkinson, H. L., and Hanisco, T. F.: A new airborne laser-induced fluorescence instrument for in situ detection of formaldehyde throughout the troposphere and lower stratosphere, Atmos Meas Tech, 8, 541-552, 10.5194/amt-8-541-2015, 2015.

Cubison, M. J., Ortega, A. M., Hayes, P. L., Farmer, D. K., Day, D., Lechner, M. J., Brune, W. H., Apel, E., Diskin, G. S., Fisher, J. A., Fuelberg, H. E., Hecobian, A., Knapp, D. J., Mikoviny, T., Riemer, D., Sachse, G. W., Sessions, W., Weber, R. J., Weinheimer, A. J., Wisthaler, A., and Jimenez, J. L.: Effects of aging on organic aerosol from open biomass burning smoke in aircraft and laboratory studies, Atmos. Chem. Phys., 11, 12049-12064, https://doi.org/10.5194/acp-11-12049-2011, 2011.

Day, D. A., Wooldridge, P. J., Dillon, M. B., Thornton, J. A., and Cohen, R. C.: A thermal dissociation laser-induced fluorescence instrument for in situ detection of NO2, peroxy nitrates, alkyl nitrates, and HNO3, J Geophys Res-Atmos, 107, Artn 4046 10.1029/2001jd000779, 2002.

de Vries, M. J. M. P., Beirle, S., Hormann, C., Kaiser, J. W., Stammes, P., Tilstra, L. G., Tuinder, O. N. E., and Wagner, T.: A global aerosol classification algorithm incorporating multiple satellite data sets of aerosol and trace gas abundances, Atmos Chem Phys, 15, 10597-10618, 10.5194/acp-15-10597-2015, 2015.

DeCarlo, P. F., Kimmel, J. R., Trimborn, A., Northway, M. J., Jayne, J. T., Aiken, A. C., Gonin, M., Fuhrer, K., Horvath, T., Docherty, K. S., Worsnop, D. R., and Jimenez, J. L.: Field-deployable, high-resolution, time-of-flight aerosol mass spectrometer, Anal Chem, 78, 8281-8289, 10.1021/ac061249n, 2006.

DeCarlo, P. F., Ulbrich, I. M., Crounse, J., de Foy, B., Dunlea, E. J., Aiken, A. C., Knapp, D., Weinheimer, A. J., Campos, T., Wennberg, P. O., and Jimenez, J. L.: Investigation of the sources and processing of organic aerosol over the Central Mexican Plateau from aircraft measurements during MILAGRO, Atmos. Chem. Phys., 10, 5257-5280, https://doi.org/10.5194/acp-10-5257-2010, 2010.

Drewnick, F., Hings, S. S., DeCarlo, P., Jayne, J. T., Gonin, M., Fuhrer, K., Weimer, S., Jimenez, J. L., Demerjian, K. L., Borrmann, S., and Worsnop, D. R.: A new time-of-flight aerosol mass spectrometer (TOF-AMS) - Instrument description and first field deployment, Aerosol Sci Tech, 39, 637-658, 10.1080/02786820500182040, 2005.

Dunlea, E. J., DeCarlo, P. F., Aiken, A. C., Kimmel, J. R., Peltier, R. E., Weber, R. J., Tomlinson, J., Collins, D. R., Shinozuka, Y., McNaughton, C. S., Howell, S. G., Clarke, A. D., Emmons, L. K., Apel, E. C., Pfister, G. G., van Donkelaar, A., Martin, R. V., Millet, D. B., Heald, C. L., and Jimenez, J. L.: Evolution of Asian aerosols during transpacific transport in INTEX-B, Atmos Chem Phys, 9, 7257-7287, DOI 10.5194/acp-9-7257-2009, 2009.

Edgerton, E. S., Hartsell, B. E., Saylor, R. D., Jansen, J. J., Hansen, D. A., and Hidy, G. M.: The Southeastern Aerosol Research and Characterization Study, part 3: Continuous measurements of fine particulate matter mass and composition, J Air Waste Manage, 56, 1325-1341, Doi 10.1080/10473289.2006.10464585, 2006.

Forrister, H., Liu, J., Scheuer, E., Dibb, J., Ziemba, L., Thornhill, K. L., Anderson, B., Diskin, G., Perring, A. E., Schwarz, J. P., Campuzano-Jost, P., Day, D. A., Palm, B. B., Jimenez, J. L., Nenes, A., and Weber, R. J.: Evolution of brown carbon in wildfire plumes, Geophys Res Lett, 42, 4623-4630, 10.1002/2015gl063897, 2015.

Gelaro, R., McCarty, W., Suarez, M. J., Todling, R., Molod, A., Takacs, L., Randles, C. A., Darmenov, A., Bosilovich, M. G., Reichle, R., Wargan, K., Coy, L., Cullather, R., Draper, C., Akella, S., Buchard, V., Conaty, A., da Silva, A. M., Gu, W., Kim, G. K., Koster, R., Lucchesi, R., Merkova, D., Nielsen, J. E., Partyka, G., Pawson, S., Putman, W., Rienecker, M., Schubert, S. D., Sienkiewicz, M., and Zhao, B.: The Modern-Era Retrospective Analysis for Research and Applications, Version 2 (MERRA-2), J Climate, 30, 5419-5454, 10.1175/Jcli-D-16-0758.1, 2017.

Giglio, L., Randerson, J. T., and van der Werf, G. R.: Analysis of daily, monthly, and annual burned area using the fourth-generation global fire emissions database (GFED4): J. Geophys. Res.-Biogeo., 118, 317–328, https://doi.org/10.1002/jgrg.20042, 2013.

Gonzalez Abad, G. G., Liu, X., Chance, K., Wang, H., Kurosu, T. P., and Suleiman, R.: Updated Smithsonian Astrophysical Observatory Ozone Monitoring Instrument (SAO OMI) formaldehyde retrieval, Atmos Meas Tech, 8, 19-32, 10.5194/amt-8-19-2015, 2015.

Guenther, A., Karl, T., Harley, P., Wiedinmyer, C., Palmer, P. I., and Geron, C.: Estimates of global terrestrial isoprene emissions using MEGAN (Model of Emissions of Gases and Aerosols from Nature), Atmos Chem Phys, 6, 3181-3210, DOI 10.5194/acp-6-3181-2006, 2006.

Hayes, P. L., Ortega, A. M., Cubison, M. J., Froyd, K. D., Zhao, Y., Cliff, S. S., Hu, W. W., Toohey, D. W., Flynn, J. H., Lefer, B. L., Grossberg, N., Alvarez, S., Rappenglueck, B., Taylor, J. W., Allan, J. D., Holloway, J. S., Gilman, J. B., Kuster, W. C., De Gouw, J. A., Massoli, P., Zhang, X., Liu, J., Weber, R. J., Corrigan, A. L., Russell, L. M., Isaacman, G., Worton, D. R., Kreisberg, N. M., Goldstein, A. H., Thalman, R., Waxman, E. M., Volkamer, R., Lin, Y. H., Surratt, J. D., Kleindienst, T. E., Offenberg, J. H., Dusanter, S., Griffith, S., Stevens, P. S., Brioude, J., Angevine, W. M., and Jimenez, J. L.: Organic aerosol composition and sources in Pasadena, California, during the 2010 CalNex campaign, J Geophys Res-Atmos, 118, 9233-9257, 10.1002/jgrd.50530, 2013.

949 Hand, J. L., Schichtel, B. A., Malm, W. C., and Frank, N. H.: Spatial and Temporal Trends in
950 PM2.5 Organic and Elemental Carbon across the United States, Adv Meteorol, Artn 367674,
951 10.1155/2013/367674, 2013.
952
953 Hand, J. L., Schichtel, B. A., Malm, W. C., Pitchford, M., and Frank, N. H.: Spatial and seasonal
954 patterns in urban influence on regional concentrations of speciated aerosols across the United
955 States, J Geophys Res-Atmos, 119, 12832-12849, 10.1002/2014jd022328, 2014.
956
957 Hayes, P. L., Carlton, A. G., Baker, K. R., Ahmadov, R., Washenfelder, R. A., Alvarez, S.,
958 Rappenglück, B., Gilman, J. B., Kuster, W. C., de Gouw, J. A., Zotter, P., Prévôt, A. S. H.,
959 Szidat, S., Kleindienst, T. E., Offenberg, J. H., Ma, P. K., and Jimenez, J. L.: Modeling the
960 formation and aging of secondary organic aerosols in Los Angeles during CalNex 2010, Atmos.
961 Chem. Phys., 15, 5773-5801, https://doi.org/10.5194/acp-15-5773-2015, 2015.
962
963 Heald, C. L., Coe, H., Jimenez, J. L., Weber, R. J., Bahreini, R., Middlebrook, A. M., Russell, L.
964 M., Jolleys, M., Fu, T. M., Allan, J. D., Bower, K. N., Capes, G., Crosier, J., Morgan, W. T.,
965 Robinson, N. H., Williams, P. I., Cubison, M. J., DeCarlo, P. F., and Dunlea, E. J.: Exploring the
966 vertical profile of atmospheric organic aerosol: comparing 17 aircraft field campaigns with a
967 global model, Atmos Chem Phys, 11, 12673-12696, 10.5194/acp-11-12673-2011, 2011.
968
969 Heald, C. L., Goldstein, A. H., Allan, J. D., Aiken, A. C., Apel, E., Atlas, E. L., Baker, A. K.,
970 Bates, T. S., Beyersdorf, A. J., Blake, D. R., Campos, T., Coe, H., Crounse, J. D., DeCarlo, P. F.,
971 de Gouw, J. A., Dunlea, E. J., Flocke, F. M., Fried, A., Goldan, P., Griffin, R. J., Herndon, S. C.,
972 Holloway, J. S., Holzinger, R., Jimenez, J. L., Junkermann, W., Kuster, W. C., Lewis, A. C.,
973 Meinardi, S., Millet, D. B., Onasch, T., Polidori, A., Quinn, P. K., Riemer, D. D., Roberts, J. M.,
974 Salcedo, D., Sive, B., Swanson, A. L., Talbot, R., Warneke, C., Weber, R. J., Weibring, P.,
975 Wennberg, P. O., Worsnop, D. R., Wittig, A. E., Zhang, R., Zheng, J., and Zheng, W.: Total
976 observed organic carbon (TOOC) in the atmosphere: a synthesis of North American
977 observations, Atmos Chem Phys, 8, 2007-2025, 10.5194/acp-8-2007-2008, 2008.
978
979 Hidy, G. M., Blanchard, C. L., Baumann, K., Edgerton, E., Tanenbaum, S., Shaw, S., Knipping,
980 E., Tombach, I., Jansen, J., and Walters, J.: Chemical climatology of the southeastern United
981 States, 1999-2013, Atmos Chem Phys, 14, 11893-11914, 10.5194/acp-14-11893-2014, 2014.
982
983 Hodzic, A., and Jimenez, J. L.: Modeling anthropogenically controlled secondary organic
984 aerosols in a megacity: a simplified framework for global and climate models, Geosci Model
985 Dev, 4, 901-917, 10.5194/gmd-4-901-2011, 2011.
986
987 Hu, W. W., Campuzano-Jost, P., Palm, B. B., Day, D. A., Ortega, A. M., Hayes, P. L.,
988 Krechmer, J. E., Chen, Q., Kuwata, M., Liu, Y. J., de Sá, S. S., McKinney, K., Martin, S. T., Hu,
989 M., Budisulistiorini, S. H., Riva, M., Surratt, J. D., St. Clair, J. M., Isaacman-Van Wertz, G.,
990 Yee, L. D., Goldstein, A. H., Carbone, S., Brito, J., Artaxo, P., de Gouw, J. A., Koss, A.,
991 Wisthaler, A., Mikoviny, T., Karl, T., Kaser, L., Jud, W., Hansel, A., Docherty, K. S., Alexander,
992 M. L., Robinson, N. H., Coe, H., Allan, J. D., Canagaratna, M. R., Paulot, F., and Jimenez, J. L.:
993 Characterization of a real-time tracer for isoprene epoxydiols-derived secondary organic aerosol
994 (IEPOX-SOA) from aerosol mass spectrometer measurements, Atmos. Chem. Phys., 15, 11807-

11833, https://doi.org/10.5194/acp-15-11807-2015, 2015.

Hudson, P. K., Murphy, D. M., Cziczo, D. J., Thomson, D. S., de Gouw, J. A., Warneke, C., Holloway, J., Jost, J. R., and Hubler, G.: Biomass-burning particle measurements: Characteristic composition and chemical processing, J Geophys Res-Atmos, 109, Artn D23s27 10.1029/2003jd004398, 2004.

Jimenez, J. L., Canagaratna, M. R., Donahue, N. M., Prevot, A. S. H., Zhang, Q., Kroll, J. H., DeCarlo, P. F., Allan, J. D., Coe, H., Ng, N. L., Aiken, A. C., Docherty, K. S., Ulbrich, I. M., Grieshop, A. P., Robinson, A. L., Duplissy, J., Smith, J. D., Wilson, K. R., Lanz, V. A., Hueglin, C., Sun, Y. L., Tian, J., Laaksonen, A., Raatikainen, T., Rautiainen, J., Vaattovaara, P., Ehn, M., Kulmala, M., Tomlinson, J. M., Collins, D. R., Cubison, M. J., Dunlea, E. J., Huffman, J. A., Onasch, T. B., Alfarra, M. R., Williams, P. I., Bower, K., Kondo, Y., Schneider, J., Drewnick, F., Borrmann, S., Weimer, S., Demerjian, K., Salcedo, D., Cottrell, L., Griffin, R., Takami, A., Miyoshi, T., Hatakeyama, S., Shimono, A., Sun, J. Y., Zhang, Y. M., Dzepina, K., Kimmel, J. R., Sueper, D., Jayne, J. T., Herndon, S. C., Trimborn, A. M., Williams, L. R., Wood, E. C., Middlebrook, A. M., Kolb, C. E., Baltensperger, U., and Worsnop, D. R.: Evolution of Organic Aerosols in the Atmosphere, Science, 326, 1525-1529, 10.1126/science.1180353, 2009.

Jimenez, J. L., Canagaratna, M. R., Drewnick, F., Allan, J. D., Alfarra, M. R., Middlebrook, A. M., Slowik, J. G., Zhang, Q., Coe, H., Jayne, J. T., and Worsnop, D. R.: Comment on "The effects of molecular weight and thermal decomposition on the sensitivity of a thermal desorption aerosol mass spectrometer", Aerosol Sci Tech, 50, I-Xv, 10.1080/02786826.2016.1205728, 2016.

Kahn, R. A., and Gaitley, B. J.: An analysis of global aerosol type as retrieved by MISR, J Geophys Res-Atmos, 120, 4248-4281, 10.1002/2015jd023322, 2015.

Kaiser, J., Jacob, D. J., Zhu, L., Travis, K. R., Fisher, J. A., Abad, G. G., Zhang, L., Zhang, X. S., Fried, A., Crounse, J. D., St Clair, J. M., and Wisthaler, A.: High-resolution inversion of OMI formaldehyde columns to quantify isoprene emission on ecosystem-relevant scales: application to the southeast US, Atmos Chem Phys, 18, 5483-5497, 10.5194/acp-18-5483-2018, 2018.

Kaiser, J., Skog, K. M., Baumann, K., Bertman, S. B., Brown, S. B., Brune, W. H., Crounse, J. D., de Gouw, J. A., Edgerton, E. S., Feiner, P. A., Goldstein, A. H., Koss, A., Misztal, P. K., Nguyen, T. B., Olson, K. F., St Clair, J. M., Teng, A. P., Toma, S., Wennberg, P. O., Wild, R. J., Zhang, L., and Keutsch, F. N.: Speciation of OH reactivity above the canopy of an isoprene-dominated forest, Atmos Chem Phys, 16, 9349-9359, 2016.

Kiehl, J. T., and Briegleb, B. P.: The Relative Roles of Sulfate Aerosols and Greenhouse Gases in Climate Forcing, Science, 260, 311-314, DOI 10.1126/science.260.5106.311, 1993.

Kim, P. S., Jacob, D. J., Fisher, J. A., Travis, K., Yu, K., Zhu, L., Yantosca, R. M., Sulprizio, M. P., Jimenez, J. L., Campuzano-Jost, P., Froyd, K. D., Liao, J., Hair, J. W., Fenn, M. A., Butler, C. F., Wagner, N. L., Gordon, T. D., Welti, A., Wennberg, P. O., Crounse, J. D., St Clair, J. M., Teng, A. P., Millet, D. B., Schwarz, J. P., Markovic, M. Z., and Perring, A. E.: Sources,

seasonality, and trends of southeast US aerosol: an integrated analysis of surface, aircraft, and satellite observations with the GEOS-Chem chemical transport model, Atmos Chem Phys, 15, 10411-10433, 10.5194/acp-15-10411-2015, 2015.

Kroll, J. H., Ng, N. L., Murphy, S. M., Flagan, R. C., and Seinfeld, J. H.: Secondary organic aerosol formation from isoprene photooxidation, Environ Sci Technol, 40, 1869-1877, 10.1021/es0524301, 2006.

Lamarque, J. F., Bond, T. C., Eyring, V., Granier, C., Heil, A., Klimont, Z., Lee, D., Liousse, C., Mieville, A., Owen, B., Schultz, M. G., Shindell, D., Smith, S. J., Stehfest, E., Van Aardenne, J., Cooper, O. R., Kainuma, M., Mahowald, N., McConnell, J. R., Naik, V., Riahi, K., and van Vuuren, D. P.: Historical (1850-2000) gridded anthropogenic and biomass burning emissions of reactive gases and aerosols: methodology and application, Atmos Chem Phys, 10, 7017-7039, 10.5194/acp-10-7017-2010, 2010.

Lamsal, L. N., Krotkov, N. A., Celarier, E. A., Swartz, W. H., Pickering, K. E., Bucsela, E. J., Gleason, J. F., Martin, R. V., Philip, S., Irie, H., Cede, A., Herman, J., Weinheimer, A., Szykman, J. J., and Knepp, T. N.: Evaluation of OMI operational standard NO2 column retrievals using in situ and surface-based NO2 observations, Atmos Chem Phys, 14, 11587-11609, 10.5194/acp-14-11587-2014, 2014.

Lee-Taylor, J., Hodzic, A., Madronich, S., Aumont, B., Camredon, M., and Valorso, R.: Multiday production of condensing organic aerosol mass in urban and forest outflow, Atmos Chem Phys, 15, 595-615, 10.5194/acp-15-595-2015, 2015.

Levelt, P. F., Van den Oord, G. H. J., Dobber, M. R., Malkki, A., Visser, H., de Vries, J., Stammes, P., Lundell, J. O. V., and Saari, H.: The Ozone Monitoring Instrument, Ieee T Geosci Remote, 44, 1093-1101, 10.1109/Tgrs.2006.872333, 2006.

Levy, R. C., Munchak, L. A., Mattoo, S., Patadia, F., Remer, L. A., and Holz, R. E.: Towards a long-term global aerosol optical depth record: applying a consistent aerosol retrieval algorithm to MODIS and VIIRS-observed reflectance, Atmos Meas Tech, 8, 4083-4110, 10.5194/amt-8-4083-2015, 2015.

Liu, X. X., Huey, L. G., Yokelson, R. J., Selimovic, V., Simpson, I. J., Muller, M., Jimenez, J. L., Campuzano-Jost, P., Beyersdorf, A. J., Blake, D. R., Butterfield, Z., Choi, Y., Crounse, J. D., Day, D. A., Diskin, G. S., Dubey, M. K., Fortner, E., Hanisco, T. F., Hu, W. W., King, L. E., Kleinman, L., Meinardi, S., Mikoviny, T., Onasch, T. B., Palm, B. B., Peischl, J., Pollack, I. B., Ryerson, T. B., Sachse, G. W., Sedlacek, A. J., Shilling, J. E., Springston, S., St Clair, J. M., Tanner, D. J., Teng, A. P., Wennberg, P. O., Wisthaler, A., and Wolfe, G. M.: Airborne measurements of western US wildfire emissions: Comparison with prescribed burning and air quality implications, J Geophys Res-Atmos, 122, 6108-6129, 10.1002/2016jd026315, 2017.

Malm, W. C., Sisler, J. F., Huffman, D., Eldred, R. A., and Cahill, T. A.: Spatial and Seasonal Trends in Particle Concentration and Optical Extinction in the United-States, J Geophys Res-Atmos, 99, 1347-1370, Doi 10.1029/93jd02916, 1994.

1087 Malm, W. C., Schichtel, B. A., Hand, J. L., and Collett, J. L.: Concurrent Temporal and Spatial
1088 Trends in Sulfate and Organic Mass Concentrations Measured in the IMPROVE Monitoring
1089 Program, J Geophys Res-Atmos, 122, 10341-10355, 10.1002/2017jd026865, 2017.
1090
1091 Marais, E. A., Jacob, D. J., Jimenez, J. L., Campuzano-Jost, P., Day, D. A., Hu, W., Krechmer,
1092 J., Zhu, L., Kim, P. S., Miller, C. C., Fisher, J. A., Travis, K., Yu, K., Hanisco, T. F., Wolfe, G.
1093 M., Arkinson, H. L., Pye, H. O. T., Froyd, K. D., Liao, J., and McNeill, V. F.: Aqueous-phase
1094 mechanism for secondary organic aerosol formation from isoprene: application to the southeast
1095 United States and co-benefit of SO2 emission controls, Atmos Chem Phys, 16, 1603-1618,
1096 10.5194/acp-16-1603-2016, 2016.
1097
1098 Marais, E. A., Jacob, D. J., Turner, J. R., and Mickley, L. J.: Evidence of 1991-2013 decrease of
1099 biogenic secondary organic aerosol in response to SO2 emission controls, Environ Res Lett, 12,
1100 ARTN 054018
1101 10.1088/1748-9326/aa69c8, 2017.
1102
1103 McDonald, B. C., de Gouw, J. A., Gilman, J. B., Jathar, S. H., Akherati, A., Cappa, C. D.,
1104 Jimenez, J. L., Lee-Taylor, J., Hayes, P. L., McKeen, S. A., Cui, Y. Y., Kim, S. W., Gentner, D.
1105 R., Isaacman-VanWertz, G., Goldstein, A. H., Harley, R. A., Frost, G. J., Roberts, J. M.,
1106 Ryerson, T. B., and Trainer, M.: Volatile chemical products emerging as largest petrochemical
1107 source of urban organic emissions, Science, 359, 760-764, ARTN aaq0524
1108 10.1126/science.aaq0524, 2018.
1109
1110 Millet, D. B., Jacob, D. J., Boersma, K. F., Fu, T. M., Kurosu, T. P., Chance, K., Heald, C. L.,
1111 and Guenther, A.: Spatial distribution of isoprene emissions from North America derived from
1112 formaldehyde column measurements by the OMI satellite sensor, J Geophys Res-Atmos, 113,
1113 Artn D02307
1114 10.1029/2007jd008950, 2008.
1115
1116 Murphy, D. M., Cziczo, D. J., Froyd, K. D., Hudson, P. K., Matthew, B. M., Middlebrook, A.
1117 M., Peltier, R. E., Sullivan, A., Thomson, D. S., and Weber, R. J.: Single-particle mass
1118 spectrometry of tropospheric aerosol particles, J Geophys Res-Atmos, 111, Artn D23s32
1119 10.1029/2006jd007340, 2006.
1120
1121 Na, K., Kim, Y. P., and Moon, K. C.: Seasonal variation of the C-2-C-9 hydrocarbons
1122 concentrations and compositions emitted from motor vehicles in a Seoul tunnel, Atmos Environ,
1123 36, 1969-1978, Pii S1352-2310(02)00149-8
1124 Doi 10.1016/S1352-2310(02)00149-8, 2002.
1125
1126 Na, K., Moon, K. C., and Kim, Y. P.: Source contribution to aromatic VOC concentration and
1127 ozone formation potential in the atmosphere of Seoul, Atmos Environ, 39, 5517-5524,
1128 10.1016/j.atmosenv.2005.06.005, 2005.
1129
1130 Nault, B. A., Campuzano-Jost, P., Day, D. A., Schroder, J. C., Anderson, B., Beyersdorf, A. J.,
1131 Blake, D. R., Brune, W. H., Choi, Y., Corr, C. A., de Gouw, J. A., Dibb, J., DiGangi, J. P.,
1132 Diskin, G. S., Fried, A., Huey, L. G., Kim, M. J., Knote, C. J., Lamb, K. D., Lee, T., Park, T.,

Pusede, S. E., Scheuer, E., Thornhill, K. L., Woo, J.-H., and Jimenez, J. L.: Secondary Organic Aerosol Production from Local Emissions Dominates the Organic Aerosol Budget over Seoul, South Korea, during KORUS-AQ, Atmos. Chem. Phys. Discuss., https://doi.org/10.5194/acp-2018-838, in review, 2018.

Ng, N. L., Kroll, J. H., Chan, A. W. H., Chhabra, P. S., Flagan, R. C., and Seinfeld, J. H.: Secondary organic aerosol formation from m-xylene, toluene, and benzene, Atmos Chem Phys, 7, 3909-3922, DOI 10.5194/acp-7-3909-2007, 2007.

Ovadnevaite, J., Zuend, A., Laaksonen, A., Sanchez, K. J., Roberts, G., Ceburnis, D., Decesari, S., Rinaldi, M., Hodas, N., Facchini, M. C., Seinfeld, J. H., and Dowd, C. O.: Surface tension prevails over solute effect in organic-influenced cloud droplet activation, Nature, 546, 637-641, 10.1038/nature22806, 2017.

Palm, B. B., de Sa, S. S., Day, D. A., Campuzano-Jost, P., Hu, W. W., Seco, R., Sjostedt, S. J., Park, J. H., Guenther, A. B., Kim, S., Brito, J., Wurm, F., Artaxo, P., Thalman, R., Wang, J., Yee, L. D., Wernis, R., Isaacman-VanWertz, G., Goldstein, A. H., Liu, Y. J., Springston, S. R., Souza, R., Newburn, M. K., Alexander, M. L., Martin, S. T., and Jimenez, J. L.: Secondary organic aerosol formation from ambient air in an oxidation flow reactor in central Amazonia, Atmos Chem Phys, 18, 467-493, 10.5194/acp-18-467-2018, 2018.

Pope, C. A., Burnett, R. T., Thun, M. J., Calle, E. E., Krewski, D., Ito, K., and Thurston, G. D.: Lung cancer, cardiopulmonary mortality, and long-term exposure to fine particulate air pollution, Jama-J Am Med Assoc, 287, 1132-1141, DOI 10.1001/jama.287.9.1132, 2002.

Pye, H. O. T., Chan, A. W. H., Barkley, M. P., and Seinfeld, J. H.: Global modeling of organic aerosol: the importance of reactive nitrogen (NOx and NO3), Atmos Chem Phys, 10, 11261-11276, 10.5194/acp-10-11261-2010, 2010.

Pye, H. O. T., Murphy, B. N., Xu, L., Ng, N. L., Carlton, A. G., Guo, H., Weber, R., Vasilakos, P., Appel, K. W., Budisulistiorini, S. H., Surratt, J. D., Nenes, A., Hu, W., Jimenez, J. L., Isaacman-VanWertz, G., Misztal, P. K., and Goldstein, A. H.: On the implications of aerosol liquid water and phase separation for organic aerosol mass, Atmos. Chem. Phys., 17, 343-369, https://doi.org/10.5194/acp-17-343-2017, 2017.

Richter, D., Weibring, P., Walega, J. G., Fried, A., Spuler, S. M., and Taubman, M. S.: Compact highly sensitive multi-species airborne mid-IR spectrometer, Appl Phys B-Lasers O, 119, 119-131, 10.1007/s00340-015-6038-8, 2015.

Ridley, D. A., Heald, C. L., Ridley, K. J., and Kroll, J. H.: Causes and consequences of decreasing atmospheric organic aerosol in the United States, P Natl Acad Sci USA, 115, 290-295, 10.1073/pnas.1700387115, 2018.

Robinson, A. L., Donahue, N. M., Shrivastava, M. K., Weitkamp, E. A., Sage, A. M., Grieshop, A. P., Lane, T. E., Pierce, J. R., and Pandis, S. N.: Rethinking organic aerosols: Semivolatile emissions and photochemical aging, Science, 315, 1259-1262, 10.1126/science.1133061, 2007.

Ryerson, T. B., Andrews, A. E., Angevine, W. M., Bates, T. S., Brock, C. A., Cairns, B., Cohen, R. C., Cooper, O. R., de Gouw, J. A., Fehsenfeld, F. C., Ferrare, R. A., Fischer, M. L., Flagan, R. C., Goldstein, A. H., Hair, J. W., Hardesty, R. M., Hostetler, C. A., Jimenez, J. L., Langford, A. O., McCauley, E., McKeen, S. A., Molina, L. T., Nenes, A., Oltmans, S. J., Parrish, D. D., Pederson, J. R., Pierce, R. B., Prather, K., Quinn, P. K., Seinfeld, J. H., Senff, C. J., Sorooshian, A., Stutz, J., Surratt, J. D., Trainer, M., Volkamer, R., Williams, E. J., and Wofsy, S. C.: The 2010 California Research at the Nexus of Air Quality and Climate Change (CalNex) field study, J Geophys Res-Atmos, 118, 5830-5866, 10.1002/jgrd.50331, 2013.

Ryerson, T. B., Trainer, M., Holloway, J. S., Parrish, D. D., Huey, L. G., Sueper, D. T., Frost, G. J., Donnelly, S. G., Schauffler, S., Atlas, E. L., Kuster, W. C., Goldan, P. D., Hubler, G., Meagher, J. F., and Fehsenfeld, F. C.: Observations of ozone formation in power plant plumes and implications for ozone control strategies, Science, 292, 719-723, DOI 10.1126/science.1058113, 2001.

Seco, R., Karl, T., Guenther, A., Hosman, K. P., Pallardy, S. G., Gu, L. H., Geron, C., Harley, P., and Kim, S.: Ecosystem-scale volatile organic compound fluxes during an extreme drought in a broadleaf temperate forest of the Missouri Ozarks (central USA), Global Change Biol, 21, 3657-3674, 10.1111/gcb.12980, 2015.

Schroder, J.C, P. Campuzano-Jost, D.A. Day, V. Shah, K. Larson, J.M. Sommers, A.P. Sullivan, T. Campos, J.M. Reeves, A. Hills, R. S. Hornbrook, N.J. Blake, E. Scheuer, H. Guo, D.L. Fibiger, E.E. McDuffie, P.L. Hayes, R.J. Weber, J.E. Dibb, E.C. Apel, L. Jaeglé, S.S. Brown, J.A. Thornton, J.L. Jimenez. Sources and Secondary Production of Organic Aerosols in the Northeastern US during WINTER. J. Geophys. Res.-Atmos., revised, 2018.

Shrivastava, M., Cappa, C. D., Fan, J. W., Goldstein, A. H., Guenther, A. B., Jimenez, J. L., Kuang, C., Laskin, A., Martin, S. T., Ng, N. L., Petaja, T., Pierce, J. R., Rasch, P. J., Roldin, P., Seinfeld, J. H., Shilling, J., Smith, J. N., Thornton, J. A., Volkamer, R., Wang, J., Worsnop, D. R., Zaveri, R. A., Zelenyuk, A., and Zhang, Q.: Recent advances in understanding secondary organic aerosol: Implications for global climate forcing, Rev Geophys, 55, 509-559, 10.1002/2016rg000540, 2017.

Solomon, P. A., Crumpler, D., Flanagan, J. B., Jayanty, R. K. M., Rickman, E. E., and McDade, C. E.: US National PM2.5 Chemical Speciation Monitoring Networks-CSN and IMPROVE: Description of networks, J Air Waste Manage, 64, 1410-1438, 10.1080/10962247.2014.956904, 2014.

Stocker, T.F., D. Qin, G.-K. Plattner, M. Tignor, S.K. Allen, J. Boschung, A. Nauels, Y. Xia, V. Bex and P.M. Midgley (eds.), IPCC, 2013: *Climate Change 2013: The Physical Science Basis. Contribution of Working Group I to the Fifth Assessment Report of the Intergovernmental Panel on Climate Change*. Cambridge University Press, Cambridge, United Kingdom and New York, NY, USA, 1535 pp, doi:10.1017/CBO9781107415324.

Taylor, K. E., and Penner, J. E.: Response of the Climate System to Atmospheric Aerosols and

Greenhouse Gases, Nature, 369, 734-737, DOI 10.1038/369734a0, 1994.

Tong, D. Q., Lamsal, L., Pan, L., Ding, C., Kim, H., Lee, P., Chai, T. F., Pickering, K. E., and Stajner, I.: Long-term NOx trends over large cities in the United States during the great recession: Comparison of satellite retrievals, ground observations, and emission inventories, Atmos Environ, 107, 70-84, 10.1016/j.atmosenv.2015.01.035, 2015.

Toon, O. B., Maring, H., Dibb, J., Ferrare, R., Jacob, D. J., Jensen, E. J., Luo, Z. J., Mace, G. G., Pan, L. L., Pfister, L., Rosenlof, K. H., Redemann, J., Reid, J. S., Singh, H. B., Thompson, A. M., Yokelson, R., Minnis, P., Chen, G., Jucks, K. W., and Pszenny, A.: Planning, implementation, and scientific goals of the Studies of Emissions and Atmospheric Composition, Clouds and Climate Coupling by Regional Surveys (SEAC(4)RS) field mission, J Geophys Res-Atmos, 121, 4967-5009, 10.1002/2015jd024297, 2016.

Torres, O., Tanskanen, A., Veihelmann, B., Ahn, C., Braak, R., Bhartia, P. K., Veefkind, P., and Levelt, P.: Aerosols and surface UV products from Ozone Monitoring Instrument observations: An overview, J Geophys Res-Atmos, 112, Artn D24s47 10.1029/2007jd008809, 2007.

Travis, K. R., Jacob, D. J., Fisher, J. A., Kim, P. S., Marais, E. A., Zhu, L., Yu, K., Miller, C. C., Yantosca, R. M., Sulprizio, M. P., Thompson, A. M., Wennberg, P. O., Crounse, J. D., St Clair, J. M., Cohen, R. C., Laughner, J. L., Dibb, J. E., Hall, S. R., Ullmann, K., Wolfe, G. M., Pollack, I. B., Peischl, J., Neuman, J. A., and Zhou, X. L.: Why do models overestimate surface ozone in the Southeast United States?, Atmos Chem Phys, 16, 13561-13577, 10.5194/acp-16-13561-2016, 2016.

Tsigaridis, K., Daskalakis, N., Kanakidou, M., Adams, P. J., Artaxo, P., Bahadur, R., Balkanski, Y., Bauer, S. E., Bellouin, N., Benedetti, A., Bergman, T., Berntsen, T. K., Beukes, J. P., Bian, H., Carslaw, K. S., Chin, M., Curci, G., Diehl, T., Easter, R. C., Ghan, S. J., Gong, S. L., Hodzic, A., Hoyle, C. R., Iversen, T., Jathar, S., Jimenez, J. L., Kaiser, J. W., Kirkevag, A., Koch, D., Kokkola, H., Lee, Y. H., Lin, G., Liu, X., Luo, G., Ma, X., Mann, G. W., Mihalopoulos, N., Morcrette, J. J., Muller, J. F., Myhre, G., Myriokefalitakis, S., Ng, N. L., O'Donnell, D., Penner, J. E., Pozzoli, L., Pringle, K. J., Russell, L. M., Schulz, M., Sciare, J., Seland, O., Shindell, D. T., Sillman, S., Skeie, R. B., Spracklen, D., Stavrakou, T., Steenrod, S. D., Takemura, T., Tiitta, P., Tilmes, S., Tost, H., van Noije, T., van Zyl, P. G., von Salzen, K., Yu, F., Wang, Z., Wang, Z., Zaveri, R. A., Zhang, H., Zhang, K., Zhang, Q., and Zhang, X.: The AeroCom evaluation and intercomparison of organic aerosol in global models, Atmos Chem Phys, 14, 10845-10895, 10.5194/acp-14-10845-2014, 2014.

Veefkind, J. P., Boersma, K. F., Wang, J., Kurosu, T. P., Krotkov, N., Chance, K., and Levelt, P. F.: Global satellite analysis of the relation between aerosols and short-lived trace gases, Atmos Chem Phys, 11, 1255-1267, 10.5194/acp-11-1255-2011, 2011.

Wagner, N. L., Brock, C. A., Angevine, W. M., Beyersdorf, A., Campuzano-Jost, P., Day, D., de Gouw, J. A., Diskin, G. S., Gordon, T. D., Graus, M. G., Holloway, J. S., Huey, G., Jimenez, J. L., Lack, D. A., Liao, J., Liu, X., Markovic, M. Z., Middlebrook, A. M., Mikoviny, T., Peischl,

J., Perring, A. E., Richardson, M. S., Ryerson, T. B., Schwarz, J. P., Warneke, C., Welti, A., Wisthaler, A., Ziemba, L. D., and Murphy, D. M.: In situ vertical profiles of aerosol extinction, mass, and composition over the southeast United States during SENEX and SEAC(4)RS: observations of a modest aerosol enhancement aloft, Atmos Chem Phys, 15, 7085-7102, 10.5194/acp-15-7085-2015, 2015.

Walgraeve, C., Demeestere, K., Dewulf, J., Zimmermann, R., and Van Langenhove, H.: Oxygenated polycyclic aromatic hydrocarbons in atmospheric particulate matter: Molecular characterization and occurrence, Atmos Environ, 44, 1831-1846, 10.1016/j.atmosenv.2009.12.004, 2010.

Warneke, C., de Gouw, J. A., Stohl, A., Cooper, O. R., Goldan, P. D., Kuster, W. C., Holloway, J. S., Williams, E. J., Lerner, B. M., McKeen, S. A., Trainer, M., Fehsenfeld, F. C., Atlas, E. L., Donnelly, S. G., Stroud, V., Lueb, A., and Kato, S.: Biomass burning and anthropogenic sources of CO over New England in the summer 2004, J Geophys Res-Atmos, 111, Artn D23s15 10.1029/2005jd006878, 2006.

Warneke, C., Veres, P., Holloway, J. S., Stutz, J., Tsai, C., Alvarez, S., Rappenglueck, B., Fehsenfeld, F. C., Graus, M., Gilman, J. B., and de Gouw, J. A.: Airborne formaldehyde measurements using PTR-MS: calibration, humidity dependence, inter-comparison and initial results, Atmos Meas Tech, 4, 2345-2358, 10.5194/amt-4-2345-2011, 2011.

Weibring, P., Richter, D., Fried, A., Walega, J. G., and Dyroff, C.: Ultra-high-precision mid-IR spectrometer II: system description and spectroscopic performance, Appl Phys B-Lasers O, 85, 207-218, 10.1007/s00340-006-2300-4, 2006.

Wolfe, G. M., Kaiser, J., Hanisco, T. F., Keutsch, F. N., de Gouw, J. A., Gilman, J. B., Graus, M., Hatch, C. D., Holloway, J., Horowitz, L. W., Lee, B. H., Lerner, B. M., Lopez-Hilifiker, F., Mao, J., Marvin, M. R., Peischl, J., Pollack, I. B., Roberts, J. M., Ryerson, T. B., Thornton, J. A., Veres, P. R., and Warneke, C.: Formaldehyde production from isoprene oxidation across NOx regimes, Atmos Chem Phys, 16, 2597-2610, 10.5194/acp-16-2597-2016, 2016.

Worton, D.R., J.D. Surratt, B.W. Lafranchi, A.W.H. Chan, Y. Zhao, R. Weber, J. Park, J.B. Gilman, J. de Gouw, C. Park, G. Schade, M. Beaver, J. StClair, J. Crounse, P. Wennberg, G. Wolfe, S. Harrold, J. Thornton, D. K. Farmer, K.S. Docherty, Mi.J. Cubison, J.L. Jimenez, A. Frossard, L. Russell, K. Kristensen, M. Glasius, J. Mao, X. Ren, W.H. Brune, E. Browne, S. Pusede, R. Cohen, J.H. Seinfeld and A.H. Goldstein. Observational Insights into Aerosol Formation from Isoprene. Environmental Science & Technology, 47, 11403-11413, doi:10.1021/es4011064, 2013.

Xu, L., Middlebrook, A. M., Liao, J., de Gouw, J. A., Guo, H. Y., Weber, R. J., Nenes, A., Lopez-Hilfiker, F. D., Lee, B. H., Thornton, J. A., Brock, C. A., Neuman, J. A., Nowak, J. B., Pollack, I. B., Welti, A., Graus, M., Warneke, C., and Ng, N. L.: Enhanced formation of isoprene-derived organic aerosol in sulfur-rich power plant plumes during Southeast Nexus, J Geophys Res-Atmos, 121, 11137-11153, 10.1002/2016jd025156, 2016.

Xu, L., Suresh, S., Guo, H., Weber, R. J., and Ng, N. L.: Aerosol characterization over the southeastern United States using high-resolution aerosol mass spectrometry: spatial and seasonal variation of aerosol composition and sources with a focus on organic nitrates, Atmos Chem Phys, 15, 7307-7336, 10.5194/acp-15-7307-2015, 2015.

Yu, K. R., Jacob, D. J., Fisher, J. A., Kim, P. S., Marais, E. A., Miller, C. C., Travis, K. R., Zhu, L., Yantosca, R. M., Sulprizio, M. P., Cohen, R. C., Dibb, J. E., Fried, A., Mikoviny, T., Ryerson, T. B., Wennberg, P. O., and Wisthaler, A.: Sensitivity to grid resolution in the ability of a chemical transport model to simulate observed oxidant chemistry under high-isoprene conditions, Atmos Chem Phys, 16, 4369-4378, 10.5194/acp-16-4369-2016, 2016.

Zhang, H. F., Yee, L. D., Lee, B. H., Curtis, M. P., Worton, D. R., Isaacman-VanWertz, G., Offenberg, J. H., Lewandowski, M., Kleindienst, T. E., Beaver, M. R., Holder, A. L., Lonneman, W. A., Docherty, K. S., Jaoui, M., Pye, H. O. T., Hu, W. W., Day, D. A., Campuzano-Jost, P., Jimenez, J. L., Guo, H. Y., Weber, R. J., de Gouw, J., Koss, A. R., Edgerton, E. S., Brune, W., Mohr, C., Lopez-Hilfiker, F. D., Lutz, A., Kreisberg, N. M., Spielman, S. R., Hering, S. V., Wilson, K. R., Thornton, J. A., and Goldstein, A. H.: Monoterpenes are the largest source of summertime organic aerosol in the southeastern United States, P Natl Acad Sci USA, 115, 2038-2043, 10.1073/pnas.1717513115, 2018.

Zhu, L., Jacob, D. J., Keutsch, F. N., Mickley, L. J., Scheffe, R., Strum, M., Abad, G. G., Chance, K., Yang, K., Rappengluck, B., Millet, D. B., Baasandorj, M., Jaegle, L., and Shah, V.: Formaldehyde (HCHO) As a Hazardous Air Pollutant: Mapping Surface Air Concentrations from Satellite and Inferring Cancer Risks in the United States, Environ Sci Technol, 51, 5650-5657, 10.1021/acs.est.7b01356, 2017.

Zhu, L., Jacob, D. J., Kim, P. S., Fisher, J. A., Yu, K., Travis, K. R., Mickley, L. J., Yantosca, R. M., Sulprizio, M. P., De Smedt, I., Abad, G. G., Chance, K., Li, C., Ferrare, R., Fried, A., Hair, J. W., Hanisco, T. F., Richter, D., Scarino, A. J., Walega, J., Weibring, P., and Wolfe, G. M.: Observing atmospheric formaldehyde (HCHO) from space: validation and intercomparison of six retrievals from four satellites (OMI, GOME2A, GOME2B, OMPS) with SEAC(4)RS aircraft observations over the southeast US, Atmos Chem Phys, 16, 13477-13490, 10.5194/acp-16-13477-2016, 2016.

Ziemann, P.J., and Atkinson, R. Kinetics, products, and mechanisms of secondary organic aerosol formation. Chem. Soc. Rev., 41, 6582-6605, doi: 10.1039/C2CS35122F, 2012.

Tables

Table 1. Linear regression parameters for OA vs. HCHO at low altitudes (<1 km)

	US (SEAC^{4}RS)	US (DC3)	US (CalNex)	South Korea (KORUS-AQ)	Wild Fires (SEAC^{4}RS)	Agricultural Fires (SEAC^{4}RS)	SEAC^{4}RS Low NO_2 and Isoprene	SEAC^{4}RS high NO_2 and Isoprene
In situ measurements OA v.s. HCHO								
Slope [a]	1.93±0.07	1.30± 0.10	1.34±0.02	2.75±0.05	25.08±0.30	3.22±0.37	2.39±0.09	1.45±0.19
Slope [b] ($\times10^{-11}$)	9.61± 0.34	6.49± 0.49	6.66±0.09	13.71 ± 0.25	125. 05 ± 1.49	16.04 ± 1.85	11.9±043	7.25±0.96
Intercept[c]	0.34±032	1.10±0.30	-0.90±0.06	1.36±0.22	−6.85±2.80	10.41±5.82	−1.14±0.37	1.14±1.22
Correlation coefficient r	0.59	0.76	0.88	0.70	0.97	0.85	0.64	0.45
GEOS- Chem model sampled along the flight track OA v.s. HCHO								
Slope[a]	1.25±0.03			1.39±0.05	0.48±0.05			
Slope ($\times10^{-11}$)	6.21± 0.14			6.95± 0.23	2.37± 0.22			
Intercept	−1.32±0.11			1.88 ± 0.07	0.12±0.03			
Correlation Coefficient r	0.76			0.43	0.53			

[a] The unit of the slope is g g^{-1}.
[b] The unit of the slope is pg $molec^{-1}$.
[c] The unit of the intercept is μg m^{-3}.
The uncertainties are one standard deviation.

Table 2. Methods to estimate OA surface concentrations, based on the choice of slope and intercept from a linear regression relationship between OA and HCHO data found in Table 1.

1[a]	Using non-BB SEAC^{4}RS relationship to represent all continental US
2[b]	Using NO_2 and isoprene dependent non-BB SEAC^{4}RS relationship for all continental US
3	Using the CalNex LA Basin relationship for large urban cites and the non-biomass burning SEAC^{4}RS relationship for other US regions
4[b]	Using the CalNex LA Basin relationship for large urban cites and the NO_2 and isoprene dependent non-BB SEAC^{4}RS relationship for other US regions

[a]SEAC^{4}RS was chosen to represent all continental US because it had the largest horizontal and vertical coverage.

[b] In methods 2 and 4, when the product of NO_2 column (Sect. 2.3) and surface isoprene emission rate (Sect. 2.4) was above threshold of 5×10^{27} molec cm^{-2} atom C cm^{-2} s^{-1}, the slope and intercept from SEAC^{4}RS high isoprene and NO_2 conditions were used. When the NO_2 column−isoprene emission product was below that threshold, the slope and intercept from SEAC^{4}RS low isoprene and NO_2 conditions were used. Threshold of "Isoprene × NO_2" is determined by its mean value over SE US (83° - 96° W and 32° - 35°N). Large urban cities are categorized with high NO_2 vertical columns (>4×10^{15} molec cm^{-2}) (Tong et al., 2015) based on the satellite NO_2 levels over LA. Isoprene emissions

instead of concentrations are used because global models use isoprene emission inventory to simulate isoprene concentrations and isoprene emission inventory is easier to access. Since isoprene has a short-lifetime of up to a few hours (Guenther et al., 2006), the emissions have a similar spatiotemporal distribution as the concentrations.

1380

1381 Figures
1382

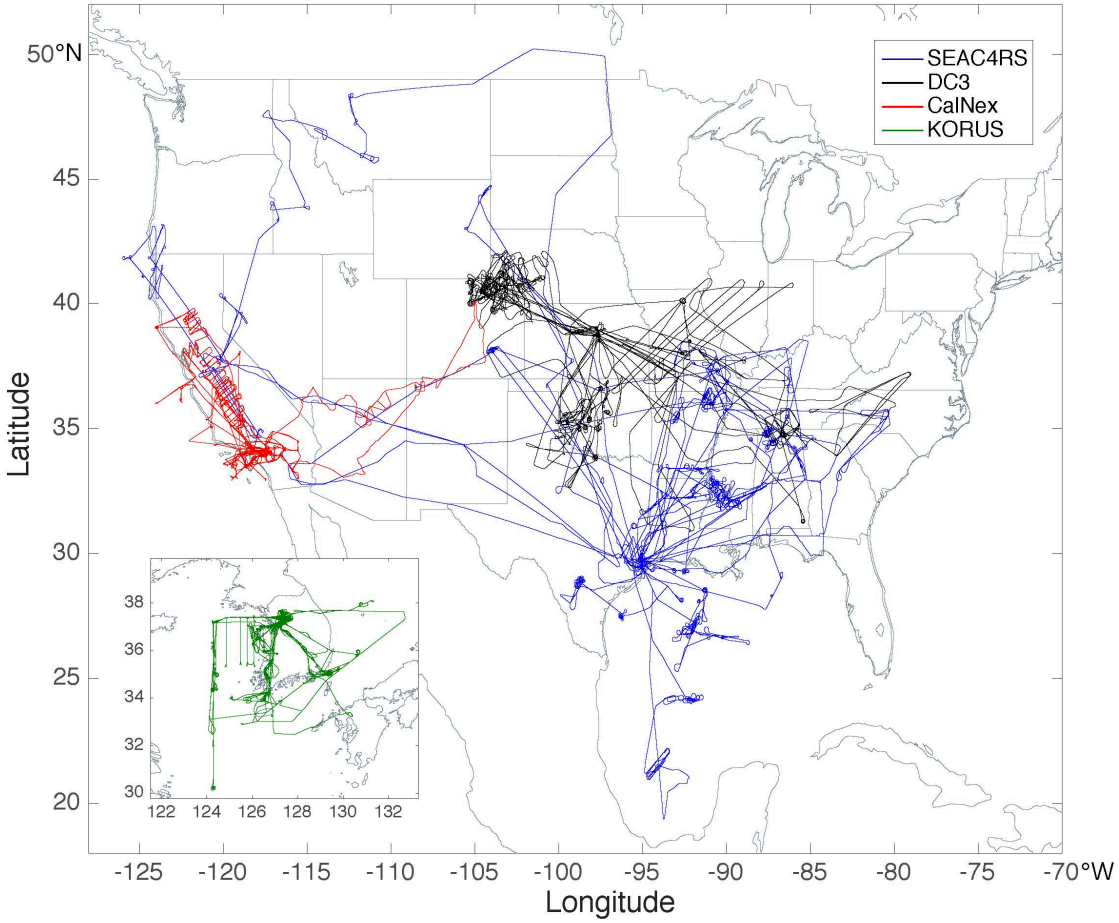

1383
1384

1385 Figure 1. Flight tracks of airborne field campaigns SEAC[4]RS (blue), DC3 (black),
1386 CalNex (red) and KORUS-AQ (green), of which in situ OA and HCHO measurements
1387 were used.
1388
1389
1390
1391

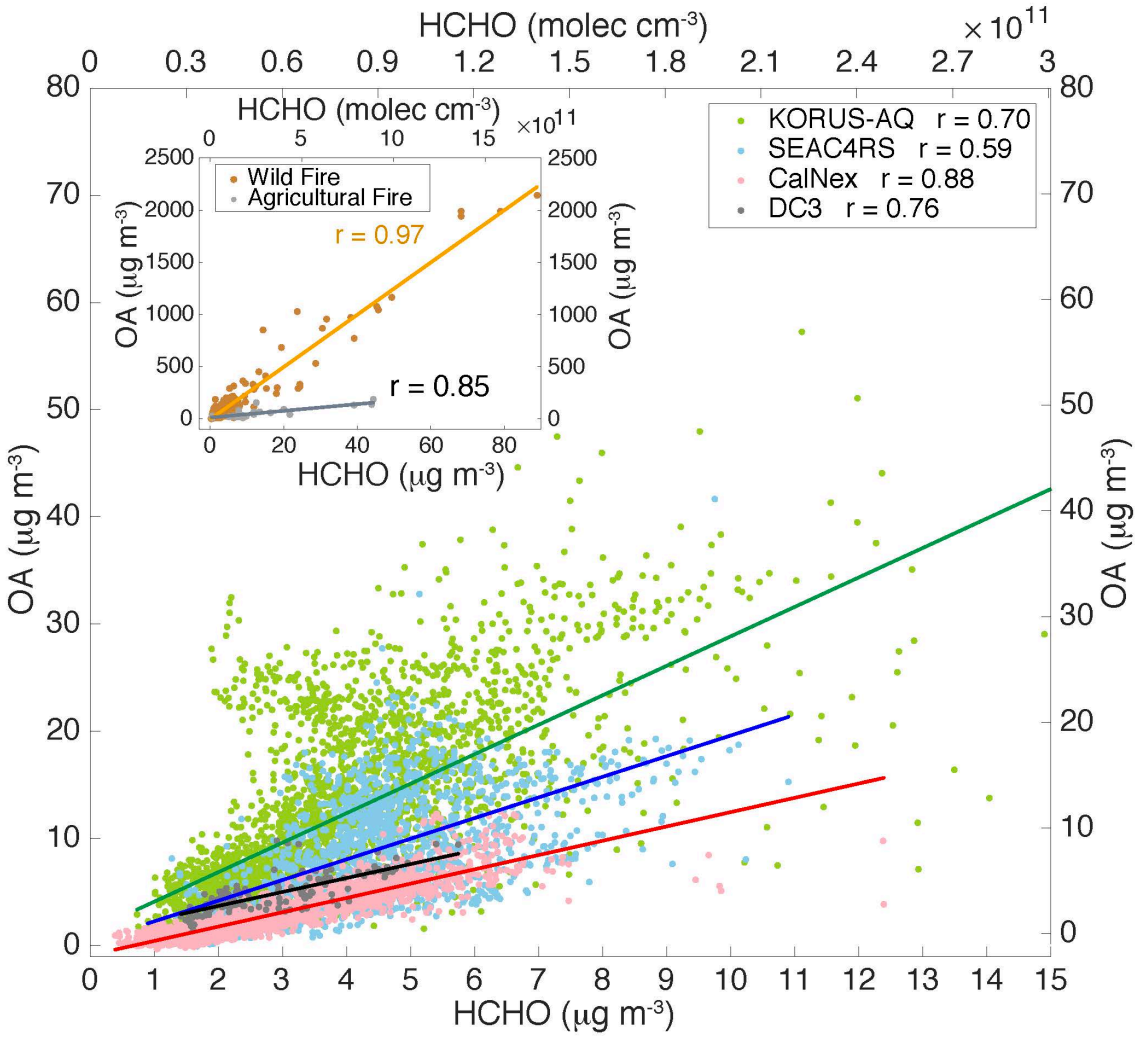

Figure 2

Scatter plots of in situ OA (µg m^{-3}) vs. HCHO (µg m^{-3} or molec cm^{-3}) from SEAC^{4}RS (excluding biomass burning) (blue), DC3 (dark grey), CalNex (pink), and KORUS-AQ (green) low altitude (< 1 km) data. Inset shows wildfire (brown), and agricultural fire (grey) SEAC^{4}RS data. SEAC^{4}RS biomass burning cases are defined as acetonitrile > 200 pptv. The linear regression fits are shown as the darker lines and correlation coefficients are provided.

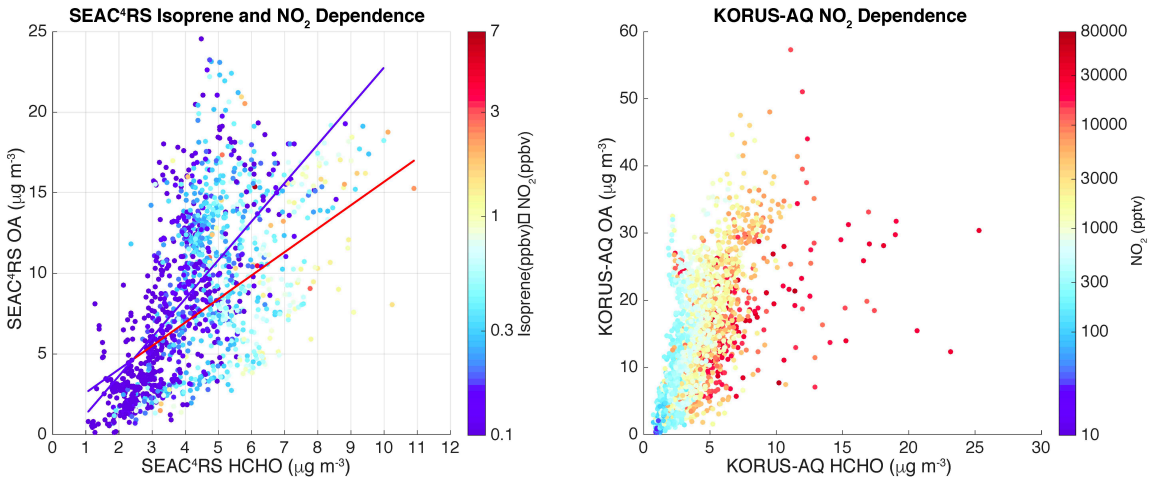

Figure 3. (a) A scatter plot of OA vs. HCHO for SEAC^{4}RS non-biomass burning low altitude data color-coded with the product of NO_2 and isoprene in log scale. The red and blue lines are the linear regression fits of high (> 0.5) and low (<0.5) product of NO_2 (ppbv) and isoprene (ppbv), respectively. (b) A scatter plot of OA vs. HCHO for KORUS-AQ data color-coded by log(NO_2).

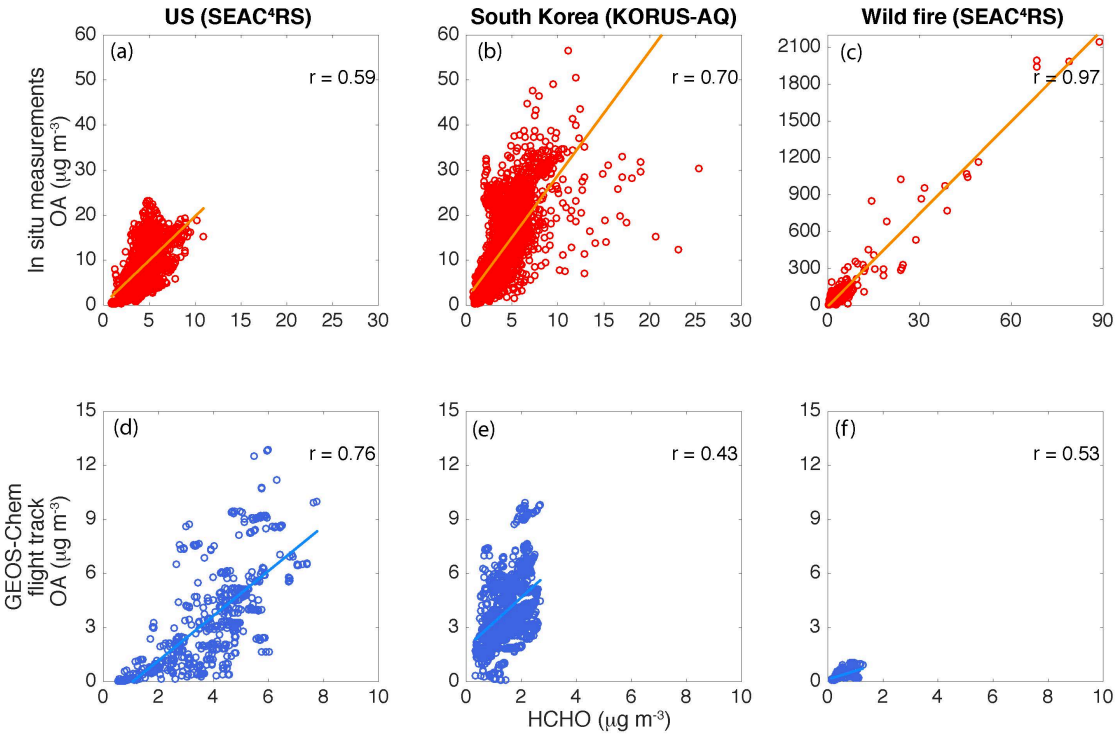

Figure 4 Scatter plots of OA vs. HCHO for US (SEAC^{4}RS altitude < 1 km non-biomass burning), South Korea (KORUS-AQ altitude < 1 km) and wildfire (SEAC^{4}RS) from in situ measurements (a, b, c) and GEOS-Chem outputs sampled along the flight tracks (d,e,f).

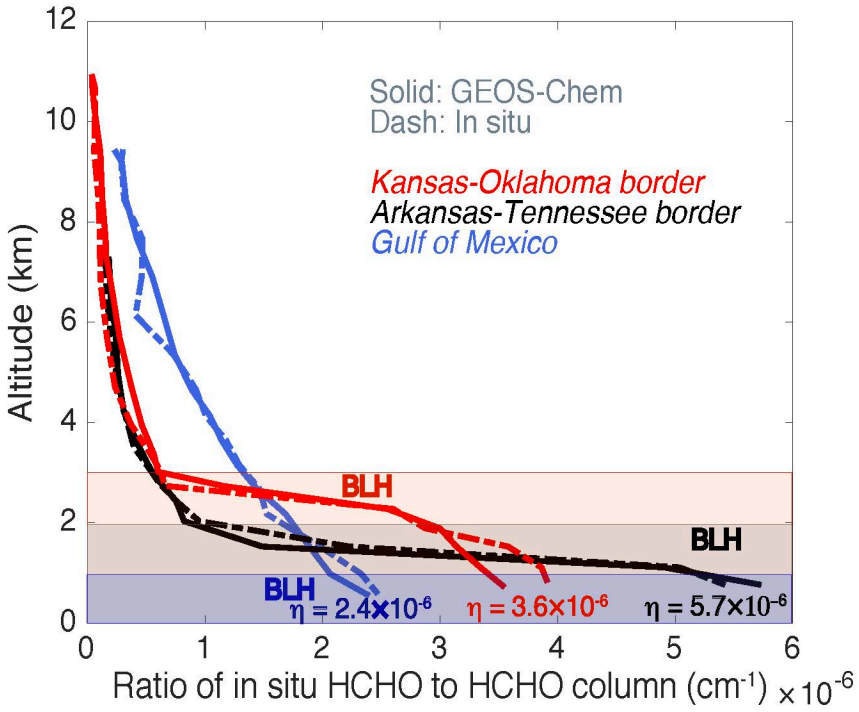

Figure 5. Three typical vertical profiles of the ratio of in situ HCHO concentrations (molec cm^{-3}) to integrated HCHO column from SEAC^{4}RS flight track. These three profiles were located at Kansas-Oklahoma border (red), Arkansas-Tennessee border (black), and Gulf of Mexico (blue). Solid curves were from GEOS-Chem results and the dashed were from ISAF measurements. HCHO columns were integrated HCHO concentrations of these vertical profiles extrapolated from 0 to 10 km, assuming the HCHO below and above the measured HCHO vertical profiles were the same as the HCHO at the lowest and highest altitudes sampled, respectively. The boundary layer heights (BLH) of these three profiles were plotted by the shaded areas.

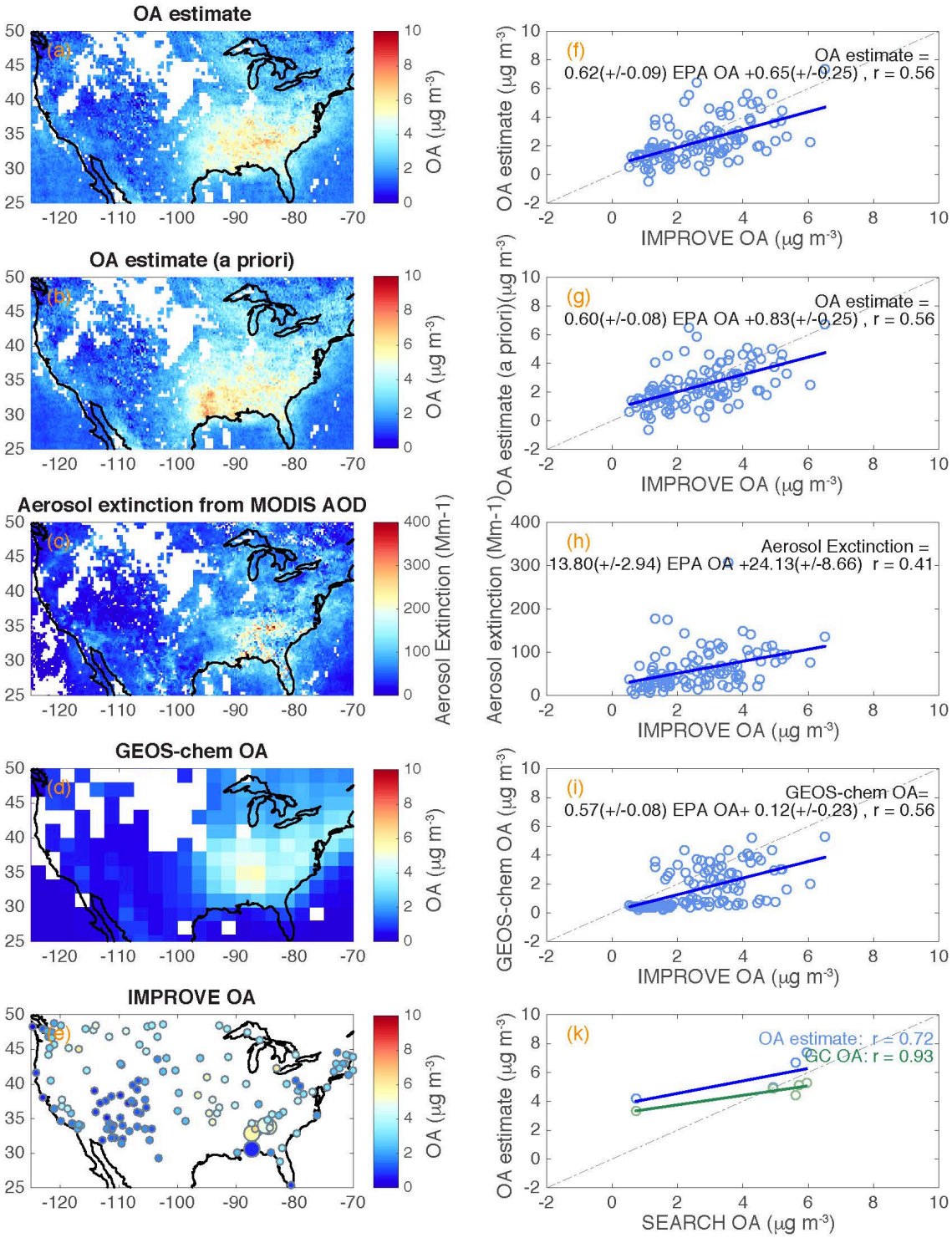

Figure 6. (a) The maps of (a) surface OA estimate (Case 1) with η from GEOS-Chem v9-02, (b) surface OA estimate (Case 1) with η from a priori profiles, (c) surface aerosol extinction derived from MODIS AOD, (d) GEOS-Chem simulated surface OA, and (e) EPA IMPROVE (small dots) and SEARCH (large dots) network ground sites color coded with OA concentrations for August 2013. The scatter plots of (f,g) surface OA estimate, (h) surface aerosol extinction derived from MODIS AOD, and (i) surface GEOS-Chem

OA vs. EPA IMPROVE network ground sites OA. IMPROVE sites OA were corrected for evaporation. (k) The scatter plots of surface OA estimate and GEOS-Chem OA vs. SEARCH network ground sites OA for August 2013. GEOS-Chem OA and OA estimate did not have good correlations with SEARCH OA for other years (SI). For the scatter plots, linear regressions are shown (blue and green lines) and regression equations and correlation coefficients for the scatter plots are listed. The dashed lines in the scatter plots indicate the 1 : 1 line. Biomass burning data (UV aerosol index > 1.6) were excluded in all panels.

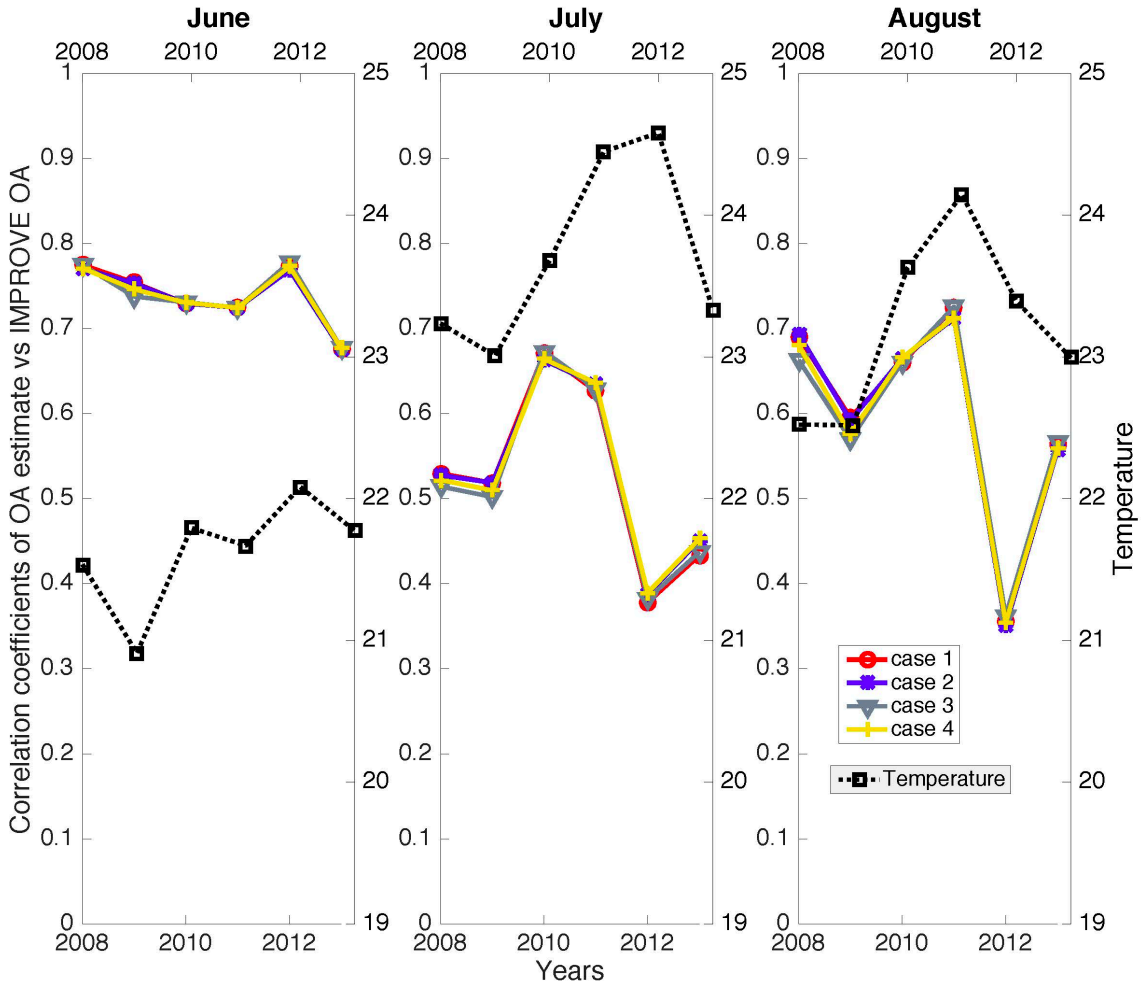

Figure 7. The correlation coefficients of the linear regression between the OA estimate from 4 cases (red, blue, gray, and yellow) vs. EPA-corrected OA from 2008 – 2013 for June, July, and August. The monthly average ambient temperature is in black.